OPTIMIZING INTEL OPTANE DC PERSISTENT MEMORY PERFORMANCE
FOR SERVERLESS STORAGE

by

Rafael Alejandro Madrid Rivera
A Thesis
Submitted to the
Graduate Faculty
of
George Mason University
In Partial fulfillment of
The Requirements for the Degree
of
Master of Science
Computer Science

Committee:

_____   Dr. Yue Cheng, Thesis Director

_____   Dr. Fei Li, Committee Member

_____   Dr. Hakan Aydin, Committee Member

_____   Dr. David Rosenblum, Department Chair

_____   Dr. Robert Pettit, Associate Chair

Date: _____   Spring Semester 2024
                                   George Mason University
                                   Fairfax, VA

Optimizing Intel Optane DC Persistent Memory Performance for Serverless Storage

A thesis submitted in partial fulfillment of the requirements for the degree of
Master of Science at George Mason University

By

Rafael Alejandro Madrid Rivera
Bachelor of Science
Central American Technological University, 2013

Director: Dr. Yue Cheng, Professor
Department of Computer Science

Spring Semester 2024
George Mason University
Fairfax, VA

Dedication

I dedicate this dissertation to ...

Acknowledgments

I would like to thank the following people who made this possible ...

Table of Contents

List of Tables

List of Figures

Abstract

OPTIMIZING INTEL OPTANE DC PERSISTENT MEMORY PERFORMANCE FOR SERVERLESS STORAGE

Rafael Alejandro Madrid Rivera, MS

George Mason University, 2024

Thesis Director: Dr. Yue Cheng

Intel Optane DC Persistent Memory (Optane PMem) presents a promising solution for developing a serverless storage service. Leveraging its unique attributes of persistence, substantial capacity, and memory-like speeds, this innovative technology holds potential to serve as efficient storage media, offering low latency and high throughput for a variety of applications running on serverless platforms. However, the dynamic and unpredictable characteristics inherent in serverless computing workloads pose challenges to the effective utilization of Optane PMem.

This thesis delves into the utilization of Optane PMem as storage media for serverless computing workloads. Through simulations of real-world serverless applications with diverse workload characteristics and performance requirements, we analyze the limitations of Optane PMem and their impact on latency and throughput service-level agreement (SLA) metrics. Our findings reveal that concurrent execution of applications sharing persistent memory leads to performance degradation and unpredictable behavior from Optane PMem. Moreover, these limitations pose contractual challenges for cloud providers, affecting their ability to meet SLAs.

To tackle these challenges, this work introduces the Non-Volatile Memory (NVM) Middleware, an optimization layer designed to enhance the efficient utilization of Optane PMem within a serverless computing environment. Seamlessly integrated with serverless storage services, the NVM Middleware assumes responsibility for Optane PMem optimization, thereby alleviating cloud providers of such burdens. Aligned with the objectives of an efficient serverless storage service, the NVM Middleware controls the concurrency level on Optane PMem, ensuring performance isolation among co-located applications. Furthermore, leveraging Reinforcement Learning (RL), an agent is trained to dynamically adjust the concurrency level applied by the NVM Middleware in response to changing workloads, enabling cloud providers to meet performance service level agreements even under shifting workloads.

Our evaluation demonstrates that the concurrency control mechanism implemented by the NVM Middleware enhances both latency and throughput exhibited by Optane PMem compared to scenarios lacking concurrency control, resulting in more predictable performance overall. Additionally, our findings indicate that employing an RL agent to dynamically tune resources within the NVM Middleware in response to changing workloads surpasses static resource allocation strategies.

Chapter 1: Introduction

1.1 Motivation

Serverless computing has experienced significant growth in recent years, emerging as a prominent paradigm for cloud application development. In serverless architecture, developers package their code into stateless functions and deploy it on the serverless platform without the responsibility of managing underlying infrastructure. The serverless platform dynamically scales resources to execute these tasks, billing users only for the resources consumed during function invocations. These characteristics make serverless computing attractive for a diverse range of applications, including web and IoT microservices [1], video processing [2], data analytics [3–5], machine learning [6,7], and storage applications [8,9].

Statelessness is a fundamental aspect of serverless functions, as they do not retain state between invocations [9]. This intentional design choice contributes to high elasticity by eliminating the need to store state within function instances. It enables cloud providers to execute functions in parallel, thereby optimizing resource utilization. Any required data between function invocations must be stored remotely, adhering to the stateless nature of serverless architecture.

While the stateless nature of serverless computing is crucial for achieving high elasticity, it imposes limitations on the types of applications that can efficiently operate on serverless platforms. Previous studies [1, 9, 10] have identified that data-intensive applications, including data analytics, machine learning workflows, and databases, face challenges due to capacity and performance gaps in existing storage services. For instance, object storage services like AWS S3 offer cost-effective long-term storage but suffer from high access latencies. Conversely, in-memory clusters like AWS ElastiCache boast low access latencies and high throughput but are costly and lack transparent provisioning. Meanwhile, key-value

databases such as AWS DynamoDB deliver high throughput but are expensive and slow to scale.

Given the constraints of current storage solutions, prior research emphasizes the necessity for a serverless storage service capable of accommodating a diverse array of workloads on serverless platforms. These studies underscore three essential requirements for such a service. Firstly, it must offer low latency and high throughput for various object sizes and data access patterns. Secondly, it should feature transparent provisioning and scalability to accommodate workload fluctuations. Finally, it is imperative that the serverless storage service guarantees isolation and predictable performance across applications and tenants to align with the requirements outlined in service level agreements (SLAs) [5, 9].

To address the requirements outlined in prior research for a serverless storage service, this study focuses on leveraging DC Persistent Memory (Optane PMem) technology. Optane PMem represents a significant advancement in non-volatile memory, offering a blend of persistence and high performance [11]. Installed on the memory bus alongside traditional DRAM, Optane PMem provides a byte-addressable interface and achieves speeds comparable to DRAM, albeit slightly slower. However, its distinguishing feature lies in its higher capacities and ability to retain data during system shutdowns or power loss, effectively functioning as persistent storage with memory-like speeds [12, 13].

This unique combination of characteristics positions Optane PMem as an ideal solution for accelerating data-intensive workloads in serverless platforms. Therefore, this thesis analyzes the efficient utilization of Optane PMem for developing a serverless storage service that meets the requirements of low latency, high throughput, transparent provisioning, scalability, and performance predictability across applications and tenants, as outlined in service level agreements (SLAs).

1.2 Research Questions

With the introduction of Optane PMem, researchers have delved into understanding its characteristics, capabilities, and limitations [12–14]. Initial expectations presumed that

2

Optane PMem would behave similarly to DRAM but with lower performance (higher latency and lower bandwidth). However, recent studies suggest that it should not be regarded simply as a "slower, persistent DRAM". Unlike DRAM, Optane PMem displays complex behaviors, and its performance varies based on factors such as access size, access type (read vs. write), and concurrency levels.

One significant difference between Optane PMem and DRAM is that Optane PMem's performance does not scale with higher thread count. This disparity stems from the mismatch between the CPU cacheline access granularity (64-byte) and the 3D-XPoint media access granularity (256-byte) in Optane PMem DIMMs. To address this discrepancy, Optane PMem DIMMs implement a small write-combining buffer to merge small writes and reduce write amplification. However, the buffer's limited capacity (16 KB) can lead to contention within the device, restricting its ability to handle access from multiple threads simultaneously.

The limited capability of Optane PMem to handle simultaneous accesses from multiple threads presents intriguing challenges for constructing a serverless storage service. In such services, resources are typically shared among tenants to execute their applications, which vary considerably in terms of data access and processing methods, as well as performance requirements. These workloads can experience significant spikes in demand, resulting in hundreds or thousands of tasks attempting to access Optane PMem concurrently. Furthermore, FaaS workloads are inherently unstable and can undergo dramatic changes over time [5, 9]. Understanding how these large-scale variations impact the performance of Optane PMem is crucial for developing an efficient serverless storage service based on this technology.

Given the wide heterogeneity of applications running on serverless platforms, we focus our work on two main types of applications: interactive and batch applications. Interactive applications, such as web-based platforms, facilitate real-time interactions between users and applications. Low latency is crucial to ensure prompt processing of user input and

delivery of real-time feedback. Conversely, batch applications, such as data analytics jobs, prioritize high throughput to efficiently process large volumes of data.

Consequently, this thesis addresses the following research questions:

- What is the performance degradation (in terms of latency and throughput) observed with Optane PMem when interactive and batch applications concurrently share the storage media? How does this performance degradation impact the service level agreements of serverless applications?

- How can we address the limitations of Optane PMem to maximize its efficiency when used as storage media for serverless workloads?

- How can we optimize and fine-tune Optane PMem to ensure consistent adherence to service level agreements as workload dynamics evolve over time?

1.3   Contributions

Our experiments offer valuable insights into the behavior of Optane PMem when employed as persistent storage for serverless workloads. Firstly, we observe that sharing Optane PMem among applications simulating real-world serverless interactive and batch applications leads to performance degradation, characterized by increased latency and reduced bandwidth. This outcome aligns with expectations, considering the contention issues experienced by Optane PMem with higher thread counts. Secondly, we find that the performance degradation in Optane PMem varies depending on the workload, affecting either latency or bandwidth more prominently. This discrepancy implies that certain applications may experience greater SLA impacts than others.

To address the limitations of Optane PMem, we introduce a control layer designed to optimize its utilization within serverless environments. Named the Non-Volatile Memory (NVM) Middleware, this layer integrates with storage services to manage Optane PMem access effectively, mitigating contention. The NVM Middleware implements distinct concurrency levels for interactive and batch applications, ensuring performance isolation across

different application types. Leveraging machine learning techniques, the NVM Middleware dynamically adjusts these concurrency levels to meet current demand and adapt to changing workloads. We advocate for the use of online reinforcement learning algorithms, given the evolving data access patterns typical of serverless workloads.

Our contributions can be summarized as follows:

- We conduct an experimental study that assesses the capabilities and limitations of Optane PMem as persistent storage for serverless workloads, a scenario not previously explored.

- We introduce the NVM Middleware, a control layer designed to reduce contention within Optane PMem while maintaining performance isolation among diverse application types.

- We propose a Reinforcement Learning (RL) model to train an agent capable of dynamically scaling and provisioning resources within the NVM Middleware to meet service level agreements amidst changing workloads.

- Finally, we provide empirical evidence showcasing the effectiveness of the concurrency control implemented by the NVM Middleware, along with the efficiency of the RL agent devised to adjust the NVM Middleware in response to workload fluctuations.

1.4   Structure

The structure of this research paper is outlined as follows:

Chapter 2 provides background information on Optane PMem, serverless computing, and Reinforcement Learning. It elaborates on the techniques employed for implementing the RL model within the NVM Middleware.

Chapter 3 details the work carried out on the NVM Middleware. Beginning with a discussion on the essential characteristics of proper serverless storage, the chapter describes how the NVM Middleware contributes to achieving these characteristics while ensuring

efficient utilization of DC PMem. It includes an overview of the architecture and programming interface of the NVM Middleware, followed by insights into the Reinforcement Learning model and the Q-Learning algorithm designed to train the NVM Middleware to dynamically adjust concurrency levels under shifting workloads.

Chapter 4 presents an evaluation of the NVM Middleware, encompassing an assessment of its concurrency control mechanism and the performance of the Q-Learning algorithm.

Chapter 5 explores related work in the fields of Optane PMem, serverless storage, and reinforcement learning for dynamic resource allocation. This chapter also discusses the relationship between our work and previous studies, highlighting similarities and differences.

Chapter 6 discusses limitations inherent in this study and proposes potential avenues for future research and development.

Finally, Chapter 7 concludes the research paper by summarizing the presented work and its implications.

Chapter 2: Background

This chapter offers background knowledge on the concepts pertinent to the scope of this study. Initially, we provide an overview of Intel Optane DC Persistent Memory, covering its architecture, applications, and performance characterization. Subsequently, we delve into serverless computing, providing insights into existing serverless storage solutions. Lastly, we present an overview of reinforcement learning, with a focus on the Q-learning algorithm and techniques for function approximation in Q-learning.

2.1 Intel Optane DC Persistent Memory

Intel Optane DC Persistent Memory (Optane PMem) represents a significant advancement in persistent memory technology, bridging the gap between dynamic random-access memory (DRAM) and storage devices [15]. As a result, it has been applied to speed up data-intensive workloads in both commercial and research settings, such as in-memory databases, virtualization software, and high-performance computing [16, 17]. This section provides an overview of the architecture, features, benefits, and applications of Optane PMem.

2.1.1 Overview of Optane PMem

Persistent memory, also referred to as non-volatile memory, represents a significant evolution in the memory/storage hierarchy (Figure 2.1), addressing the performance and capacity gap between dynamic random-access memory (DRAM) and traditional storage mediums. This innovative technology combines the characteristics of both DRAM and storage, offering the speed of DRAM and the non-volatile nature of storage devices [15, 19].

Optane PMem stands at the forefront of commercial implementations of persistent memory technology, leveraging Intel's innovative 3D-XPoint technology. Like DRAM, Optane

Figure 2.1: Illustration of the Memory-Storage Hierarchy with persistent pemory. Persistent memory introduces a new tier in the hierarchy, bridging the performance and capacity gap between traditional volatile memory and persistent storage. Adapted from [18].

PMem is available in the form of Dual In-line Memory Modules (DIMMs), which are directly connected to the memory bus. This direct connection enables applications to access persistent memory with the same ease as traditional DRAM, eliminating the need for frequent data transfers between memory and storage. However, unlike DRAM, Optane PMem DIMMs provide significantly greater capacity and retain data even when power is removed, thereby enhancing system performance and enabling fundamental changes in computing architecture. Upon its introduction, the Optane PMem offers substantial capacities up to 512GiB [12, 13].

Optane PMem is exclusively supported by Intel Cascade Lake platform. Each processor within this platform is equipped with two integrated memory controllers (iMCs), with each iMC supporting three channels. This architecture seamlessly integrates Optane PMem with DRAM, allowing users to deploy up to one Optane PMem per channel and up to six per CPU socket, thereby enabling extensive persistent memory capacities of potentially up to 3TiB per socket [12, 13].

Similar to conventional DRAM DIMMs, Optane PMem DIMMs are positioned on the memory bus and connect directly to the processor's iMC. The communication protocol between the iMC and the Optane PMem DIMM is depicted in Figure 2.2. Communication between the iMC and the Optane PMem DIMM occurs via the DDR-T protocol, adapted for persistent memory and operating at cache line granularity (64B). Initial memory access to the Optane PMem DIMM is coordinated by the onboard Controller, which manages access to the 3D-XPoint media. Analogous to SSDs, the Optane PMem DIMM conducts address translation for wear-leveling and bad block management, facilitated by the maintenance of an address indirection table (AIT). Following translation, access to the storage media occurs. Notably, with 3D-XPoint access granularity set at 256B, the controller converts 64-byte accesses into 256-byte accesses, inducing write amplification. To mitigate this, the controller incorporates a 16KB write-combining buffer to merge adjacent writes [12–14].
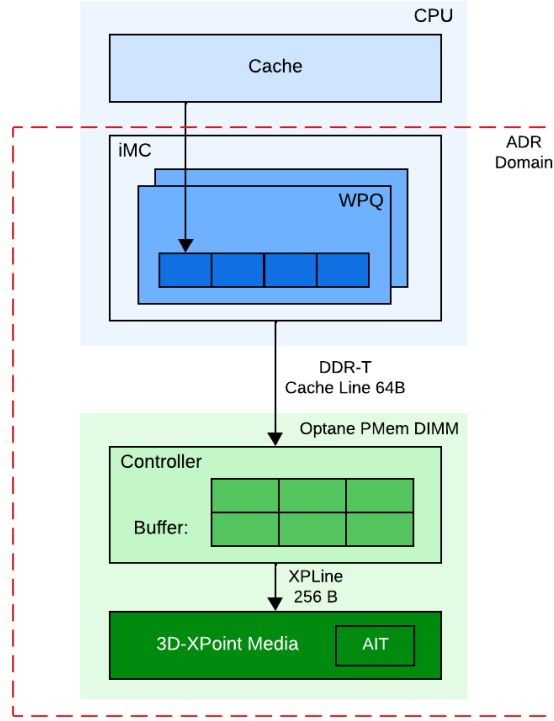
Figure 2.2: Illustration depicting the architecture of Intel Optane DC Persistent Memory. Adapted from [12].

To ensure data persistence, Intel platforms integrate the iMC and Optane PMem DIMM within the asynchronous DRAM refresh (ADR) domain. Intel's ADR feature ensures that CPU stores that reach the ADR domain will survive a power failures [12]. The iMC manages read and write pending queues for each Optane PMem DIMM, with the ADR domain encompassing the write pending queue. Once data reaches the write pending queue, ADR ensures its persistence within Optane PMem DIMM in the event of power failures. The ADR domain excludes the CPU caches, necessitating additional steps beyond simply executing a store instruction to ensure data persistence. To achieve this, CPU stores must be continually flushed using specialized instructions provided by Intel's Instruction Set Architecture (ISA), including CLFLUSH, CLFLUSHOPT, and CLWB [12, 13, 19].

2.1.2 Performance Characterization

Previous studies [12, 13] conducted an empirical performance assessment of Optane PMem, revealing its nuanced behavior compared to DRAM. They observed that Optane PMem's performance varies significantly depending on specific access patterns, including access size, type, and concurrency level. Notably, they found that Optane PMem's read latency is three times slower than that of DRAM, primarily due to Optane PMem's longer media latency. However, sequential access patterns demonstrate notably improved latency, indicating Optane PMem's capability to consolidate adjacent requests into single 256-byte accesses. The study also highlights that Optane PMem achieves a maximum random read bandwidth of 6.6 GB/s and a write bandwidth of 2.3 GB/s. Moreover, sequential access further enhances bandwidth performance, exhibiting up to a fourfold increase [12, 13].

An insightful observation highlighted by Izraelevitz et al. [13] is that Optane PMem's bandwidth can become saturated when utilized in real-world multi-threaded applications, thereby introducing performance overhead. This phenomenon arises due to Optane PMem's inability to scale performance proportionally with increased thread count, primarily due to contention occurring within the processor's iMC and Optane PMem's buffer. Contentious conditions within the buffer exacerbate the frequency of evictions and write-backs to the 3D-XPoint media, resulting in Optane PMem writing more data internally than what the application necessitates. Furthermore, given Optane PMem's slightly slower performance compared to DRAM, the slower drainage of write pending queues by Optane PMem introduces head-of-line blocking effects. As the number of threads concurrently accessing Optane PMem increases, contention on the device escalates, heightening the likelihood of the processor experiencing blocking while awaiting completion of previous store operations [12].

2.1.3 Operating Modes and Applications

Optane PMem offers two distinct operating modes: Memory mode and App Direct mode.

In Memory mode, Optane PMem serves as a high-capacity main memory without persistence. In this configuration, DRAM is concealed from users and acts solely as a cache for Optane PMem, seamlessly managed by the operating system [12].

Conversely, in App Direct mode, Optane PMem DIMMs are directly exposed to the operating system as independent persistent memory devices, thus enabling their utilization for persistent storage [13]. Functionally, the operating system perceives DRAM and Optane PMem as distinct memory pools, with the latter offering data persistence. Applications can access Optane PMem through direct load/store operations or via a file system configured with the dax (direct access) option. Such a file system is termed as a PM-aware file system, facilitating direct access to persistent memory without relying on the page cache [19, 20].

In the context of this thesis, Optane PMem is exclusively employed in App Direct Mode, coupled with a PM-aware file system to harness its storage capabilities.

2.1.4 Programming

In the realm of persistent memory technology, maintaining data consistency across runtime and system reboots is essential. To address this challenge, prior research underscores the necessity for applications leveraging persistent memory to implement transactions that are atomic, consistent, thread-safe, and resilient to system failures—a paradigm akin to ACID transactions in database systems. However, achieving such robustness in real-world scenarios poses significant complexity. Recognizing this, Intel has developed the Persistent Memory Development Kit (PMDK) to tackle this challenge [15, 19].

PMDK comprises a comprehensive suite of libraries and tools tailored for both application developers and system administrators, aiming to streamline the management and utilization of persistent memory devices. Drawing on the SNIA NVM Programming model [21] as its foundation, these libraries extend its capabilities to varying extents. Some libraries offer simplified wrappers around operating system primitives, facilitating ease of use, while others provide sophisticated data structures optimized for persistent memory usage [15].

In the scope of this thesis, we leverage PMEMKV [22], a persistent local key-value store provided by PMDK. Designed with cloud environments in mind, PMEMKV complements PMDK's suite of libraries with cloud-native support, abstracting the intricacies of programming with persistent memory through a familiar key-value API. Notably, PMEMKV distinguishes itself from traditional key-value databases by enabling direct access to data. This means that reading data from persistent memory circumvents the need for copying it into DRAM—an approach that significantly enhances the performance of applications leveraging persistent memory [15].

2.2 Serverless Computing

Serverless computing, a prominent execution model within cloud computing, revolutionizes the deployment process by allowing developers to deploy code without the need for provisioning or managing server infrastructure. Although termed "serverless," this model still utilizes servers provided by cloud vendors to execute developers' code. However, the distinguishing feature lies in the abstraction of infrastructure management from the developer's perspective. Developers no longer concern themselves with resource provisioning, scaling, fault tolerance, monitoring, or security patches; instead, they focus solely on code development. Cloud providers take on the responsibility of handling these infrastructure-related tasks on behalf of their customers. Consequently, developers are charged based on the execution time and resources consumed during their code invocations, offering a pay-per-use billing model [5, 9, 23].

At the heart of serverless computing lies Function-as-a-Service (FaaS), introduced by AWS Lambda in 2015. Since then, various commercial and open-source alternatives have emerged, including Google Cloud Functions, Azure Functions, Apache OpenWhisk, and others. FaaS enables developers to express application logic as stateless functions written in high-level languages such as Java, Python, C, or C++. These functions, known as serverless functions, are packaged together with their dependencies and submitted to the serverless platform. Additionally, developers associate events with each serverless function,

such as HTTP requests, file uploads, database triggers, and more. Upon the occurrence of an event, the cloud provider promptly executes the associated serverless function, offering a scalable and event-driven approach to application development and deployment [24–27].

2.2.1 Workload Characterization

Previous research has underscored the dynamic and unpredictable nature of FaaS workloads within serverless computing environments. Analyzing these workloads often involves examining real-world FaaS provider logs to discern patterns and characteristics. Typically, applications in serverless computing are composed of interconnected serverless functions, each serving a specific logical purpose. Cloud providers face significant challenges in predicting the next function invocation due to the diverse array of triggers employed by applications. Moreover, the heterogeneity of these applications results in substantial variations in invocation frequency, data access sizes, and usage patterns. Data access sizes can range from mere bytes to gigabytes, while invocation frequencies can span several orders of magnitude, with some functions being infrequently called. Learning the invocation patterns of rarely invoked functions is particularly challenging. Additionally, a significant portion of data accesses exhibit bursty behavior, leading to rapid surges in I/O requests as multiple function instances are dynamically spun up to meet application demands. This phenomenon often results in short-lived bursts of intense activity within applications [5, 23, 28].

2.2.2 Storage for Serverless Functions

Serverless providers enforce a restriction on direct communication between serverless functions, necessitating the adoption of remote storage mechanisms for data interchange among them [5, 9, 23].

One approach to facilitate data exchange between serverless functions is through the utilization of serverless storage, a framework within cloud computing that abstracts the intricacies of managing storage infrastructure from developers. With serverless storage, developers harness storage services provided by cloud vendors like AWS S3, Google Cloud

Storage, Azure Blob Storage, AWS DynamoDB, and others. These services empower developers to store and retrieve data via APIs or SDKs without the burden of managing servers or storage clusters. Moreover, serverless storage services offer features such as automatic scaling, data durability, and pay-per-use pricing models, enabling developers to seamlessly adjust their storage resources in line with demand without the need for upfront provisioning or capacity planning. This scalability is of paramount importance for applications characterized by fluctuating storage requirements or unpredictable workloads [29–35].

Despite the high scalability of existing serverless storage solutions, they are primarily optimized for durability rather than performance [5, 8, 9]. Studies have demonstrated that object-based storage solutions like AWS S3 may exhibit latencies of up to 10 milliseconds for small object reads or writes [36]. Similarly, key-value databases such as AWS DynamoDB, Google Cloud Datastore, and Azure Cosmos provide high throughput but may entail high expenses and lengthy scaling processes [9].

In scenarios demanding enhanced performance, developers may opt for in-memory key-value stores like AWS ElastiCache [37]. These solutions offer low access latencies and high throughput but incur higher costs associated with DRAM. Additionally, they do not provide persistence, meaning that data is not retained in the event of a system failure. However, a notable drawback is their lack of autoscaling capabilities, necessitating manual management and scaling of clusters when integrated with serverless functions [5, 8, 9].

2.2.3 Service Level Agreements

Service level agreements (SLAs) are integral to cloud storage as they establish the terms and conditions governing the quality of service between cloud providers and customers. These agreements, formalized through SLAs, represent negotiated contracts wherein both parties delineate system-related attributes, including the client's anticipated request characteristics and the expected performance of the storage service under these conditions. SLAs serve to define the repercussions for any deviation from the predetermined service levels, often entailing service credits, refunds, or other forms of redress. Such measures incentivize

providers to fulfill their obligations and redress any disruptions or deficiencies in service promptly [31, 38, 39].

In the realm of storage services, latency and throughput-related SLAs are of paramount importance. While conventional practice often involves describing performance SLAs using mean or median metrics, these measures may not adequately ensure a consistently positive user experience across all customers. Instead, a more effective approach involves assessing performance SLAs in terms of tail (99th) percentiles, thereby prioritizing the resolution of exceptional cases and optimizing service quality for all users [31].

2.3   Reinforcement Learning

Reinforcement Learning (RL) is a subfield of machine learning concerned with learning optimal decision-making policies through interactions with an environment [40].

2.3.1   Overview of Reinforcement Learning

The fundamental concept underlying RL is the notion of an agent, which takes actions in an environment and receives feedback in the form of rewards, indicating the quality of its decisions. The agent's objective is to learn a policy that maximizes cumulative rewards over time. Moreover, the agent is not provided with explicit instructions on which actions to take; instead, it must discover the actions that lead to the highest rewards by trying them.
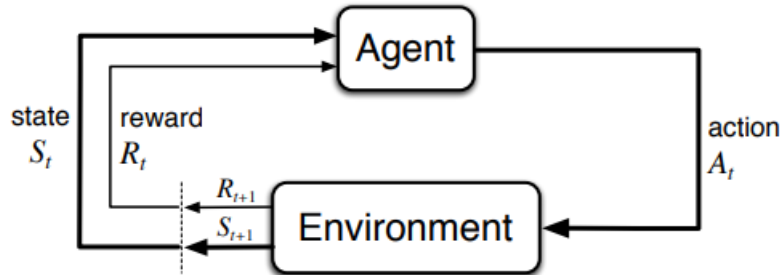
Figure 2.3: Workflow illustrating the interaction between the agent and the environment in reinforcement learning. Adapted from [40].

Figure 2.3 presents a schematic representation of a standard reinforcement learning scenario. In discrete time steps, the agent perceives the current state s_t from the set of all possible states S. It then selects an action a_t from the available actions $A(s_t)$ in the current state. The environment transitions to a new state s_{t+1}, and the agent receives a reward r_t associated with the transition (s_t, a_t, s_{t+1}).

The agent's behavior is governed by its policy, which maps perceived states to actions. The ultimate aim is to learn an optimal or near-optimal policy that maximizes the cumulative reward.

2.3.2 Q-Learning

One of the foundational algorithms in RL is Q-Learning, introduced by Watkins in 1989 [41]. The algorithm belongs to the class of model-free RL algorithms, meaning it learns directly from experience without requiring a model of the environment dynamics [42].

At the core of Q-Learning is the Q-value function, denoted as $Q(s, a)$, which represents the expected cumulative reward the agent will receive by taking action a in state s and following an optimal policy thereafter. The objective of Q-Learning is to iteratively update the Q-values based on observed transitions and rewards, eventually converging to the optimal Q-values that maximize long-term rewards.

The Q-Learning algorithm proceeds as follows: the agent interacts with the environment by selecting actions based on its current estimate of the Q-values. Upon taking an action, the agent observes the resulting reward and the next state. It then updates the Q-value of the previous state-action pair using the observed reward and the estimated value of the next state.

The Q-value update rule in Q-Learning is based on the Bellman equation, which expresses the relationship between the Q-values of successive states [42]:

$$Q(s,a) \leftarrow (1 - \alpha) \cdot Q(s,a) + \alpha \cdot \left(r + \gamma \cdot \max_{a'} Q(s', a') \right)$$

Here, α is the learning rate, determining the extent to which new information overrides the old one, and γ is the discount factor, representing the importance of future rewards relative to immediate rewards. The term $r + \gamma \cdot \max_{a'} Q(s', a')$ is known as the temporal-difference (TD) target, combining the immediate reward r with the discounted maximum Q-value of the next state s' [42].

2.3.3 Function Approximation using Regression Models

One of the key advantages of Q-Learning is its simplicity and ease of implementation. It requires only a table to store the Q-values, making it computationally efficient for small state and action spaces. However, Q-Learning faces challenges in environments with large state spaces, as maintaining a lookup table becomes infeasible due to memory and computational constraints.

Function approximation is a fundamental technique in reinforcement learning (RL) aimed at approximating the Q-Value function when dealing with large state or action spaces where tabular representations become impractical [42]. This approach allows RL agents to generalize from observed states to unseen states, facilitating decision-making in unexplored regions of the state space.

In the realm of RL, regression models serve as fundamental tools for function approximation [40]. These models, widely employed in machine learning, aim to learn the relationship between input variables (features) and a continuous target value [42]. In RL, they find application in approximating the Q-value function, represented as a weighted combination of features, with each feature encapsulating a distinct aspect of the state space. The utilization of gradient-descent techniques, notably stochastic gradient descent, facilitates iterative refinement of the parameters governing the weighted function, with the objective of minimizing a predefined loss function. Through this iterative optimization process, the model progressively enhances its predictive accuracy, enabling it to capture intricate patterns within the state-action space [40].

Regression models encompass diverse representations, including linear models, polynomial models, and neural networks [40]. Within this study, our focus centers on exploring the utility of linear or polynomial regression models for function approximation. Linear regression models presume a linear association between input features and the target variable. In contrast, polynomial regression models extend linear regression by accommodating non-linear relationships between input features and target values [43]. Particularly in environments characterized by complex dynamics or non-linear reward structures, polynomial regression models excel in capturing intricate relationships more effectively than their linear counterparts.

Hyperparameter tuning is a critical aspect of training regression models [44]. Hyperparameters, such as the learning rate, degree of polynomial, and regularization strength, significantly impact the performance and convergence of the models. A systematic approach to hyperparameter tuning involves experimenting with different combinations of hyperparameters, evaluating the performance of the trained models on a validation set, and selecting the optimal hyperparameters based on predefined criteria, such as validation error or performance metrics [42].

2.3.4 Exploration-Exploitation Tradeoff

The exploration-exploitation tradeoff poses a significant challenge in reinforcement learning [40]. The agent must strike a balance between exploring unfamiliar actions to gather information and exploiting known actions for immediate rewards. Finding this balance is crucial for effective learning and task performance, as the agent gradually favors actions with higher expected rewards.

One classic strategy for balancing exploration and exploitation is the epsilon-greedy (e-greedy) algorithm [40]. The e-greedy policy selects the action that maximizes the estimated value with probability $1 - \epsilon$ (exploitation) and selects a random action with probability ϵ (exploration). This approach ensures that the agent continues to explore the environment while gradually exploiting more rewarding actions as it gains knowledge.

Decayed e-greedy methods aim to strike a balance between exploration and exploitation by gradually reducing the exploration rate ϵ as the agent gains more experience or as the training progresses [40]. This decay encourages the agent to explore the environment more extensively in the early stages of learning while gradually shifting towards exploitation as it becomes more knowledgeable.

2.3.5 Reward shaping

Reward shaping is a technique in reinforcement learning aimed at accelerating learning by modifying the reward signal provided to the agent. Traditional RL algorithms rely solely on sparse reward signals, which can make learning slow and inefficient, especially in complex environments. Reward shaping addresses this issue by providing additional, shaped rewards that guide the agent towards desirable behaviors. These shaped rewards are designed to provide more informative feedback to the agent, encouraging it to explore the state-action space more effectively. However, reward shaping must be carefully designed to avoid unintended consequences such as overfitting to the shaped rewards or incentivizing undesirable behaviors [42].

Chapter 3: Optimizing Optane PMem Performance for Serverless Storage

As discussed earlier, the introduction of Optane PMem presents a significant opportunity for serverless storage services. This memory technology offers a unique combination of cost-effective high capacity, high performance, and support for data persistence [11]. When utilized in App-Direct mode, Optane PMem DIMMs and DRAM DIMMs function as independent memory resources directly controlled by applications for load/store operations. This configuration allows Optane PMem capacity to serve as byte-addressable persistent memory mapped into the system application space, providing direct accessibility to applications. Consequently, Optane PMem can function as persistent storage with memory-like speeds.

However, resource contention within Optane PMem can lead to substantial performance and contractual implications for multi-tenant serverless storage services. The limited capability of Optane PMem to handle accesses from multiple threads can result in degraded system performance during workload spikes, undermining the hallmark autoscaling features of serverless computing. Moreover, in multi-user environments, where physical resources are shared among tenants, performance variations due to Optane PMem contention can hinder service providers from offering consistent service level agreements.

To mitigate contention effects, prior research recommends restricting the number of threads accessing Optane PMem simultaneously. For instance, Yang et al. [12] enhanced the performance of an PM-aware file system by limiting the number of writer threads accessing each Optane PMem DIMM. Similarly, Ribbon [14] dynamically adjusts the number of threads performing cache line flushing (CLF) operations at runtime. While effective, such approaches introduce management complexities for system administrators managing multi-tenant serverless storage environments.

Given the intricate nature of FaaS workloads, implementing efficient concurrency control mechanisms to optimize an Optane PMem-based serverless storage service is challenging. These challenges are elaborated in Section 3.1, but, in summary, service providers face three key tasks: ensuring predictable performance to meet diverse SLAs, transparently scaling resources to match current workload demands, and swiftly adapting to sudden workload shifts. To address these challenges, we propose a solution that shoulders these responsibilities on behalf of service providers.

This chapter introduces the NVM Middleware, a middleware optimization layer positioned between a serverless storage service and Intel Optane PMem. Its primary objective is to address the limitations associated with Optane PMem while simultaneously meeting the diverse (SLAs) required by multiple tenants amid varying workloads. Additionally, the chapter describes the development of a reinforcement learning agent to enable the NVM Middleware to quickly adapt to changing workloads. This agent considers workload characteristics and SLAs metrics, learning from past experiences to dynamically scale resources.

The subsequent sections of this chapter elaborate on the design objectives of the NVM Middleware, providing insights into its architectural principles and programming interface. Furthermore, the chapter delves into the implementation aspects of the reinforcement learning model, elucidating the training methodology employed to equip an agent with the capability to dynamically adjust the NVM Middleware's concurrency levels in response to fluctuating workloads. Lastly, the chapter provides an in-depth discussion on the implementation intricacies of the NVM Middleware.

3.1 Motivation

In this section, we discuss the pain points of controlling concurrency levels to optimize Optane PMem within a serverless storage service and explain the design goals of the NVM Middleware.

3.1.1 Concurrency Control Challenges in Serverless Storage

When building an Optane PMem-based serverless storage service, optimizing the memory's performance is just the start. Early works in serverless computing have identified several tasks that a storage service must perform efficiently to meet the demands of serverless computing [5, 9, 23, 38, 45, 46]. As a result, service providers must ensure that their concurrency control policies do not interfere with these design goals. In this work, we focus on three challenges faced by service providers when designing a high-performance storage service.

Support for a wide heterogeneity of applications

In serverless computing, applications are often deployed as a set of serverless functions that interact with remote storage for data sharing. Previous research indicates significant diversity among these applications concerning data access size [5, 23], access patterns [23], and performance requirements [9, 38]. Consequently, service providers encounter the challenge of adjusting concurrency levels to accommodate various application types. In this study, we focus on two distinct application categories: interactive applications, which prioritize low-access latency, and batch applications, which emphasize achieving high throughput.

A measurement study was conducted to evaluate the effects of concurrent interactive and batch applications sharing Optane PMem. The study utilized the applications and experimental platform detailed in Section 4. The results are illustrated in Figure 3.1. In this experiment, both an interactive application (YCSB) and a batch application (SVD) were executed individually and concurrently, utilizing Optane PMem as their storage medium. The findings illustrate a noticeable impact on both throughput and 99th latency when running the applications concurrently. Particularly, latency is significantly affected compared to throughput, suggesting contention among tenant workloads sharing Optane PMem. Hence, effective concurrency control mechanisms are essential to mitigate such contention, while reaching a balance between latency and throughput exhibited.
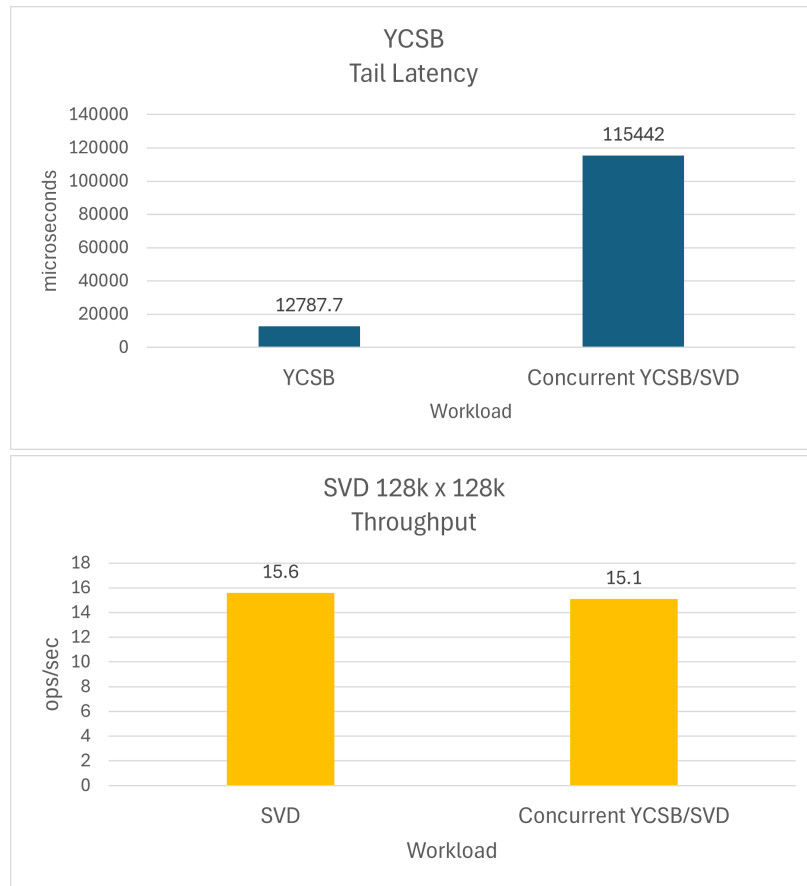
Figure 3.1: Comparison of 99th latency and throughput variations observed in Optane DC PMem when running YCSB and SVD applications concurrently. The top image depicts the latency comparison between YCSB running alone and concurrently with SVD, while the bottom image illustrates the throughput comparison between SVD running alone and concurrently with YCSB. Notably, concurrent application execution significantly impacts the 99th latency compared to throughput.

Compliance with Service Level Agreements

The success of a storage service relies on its ability to comply with various SLAs. SLAs play a critical role in governing the relationship between the storage provider and its customers. They help establish clear expectations between both parties regarding the quality of storage service. Therefore, service providers face the challenge of staying in compliance with these SLAs while they seek to optimize Optane PMem.

Automatic and transparent scaling

Serverless workloads are extremely unpredictable. These workloads can launch hundreds of functions instantaneously to meet application demands [45]. Furthermore, the data access patterns of the applications can change dramatically over time [23, 46]. Service providers face the challenge of scaling the resources, such as number of threads, automatically to meet the demands of changing workloads. In addition, they must ensure that the system adapts quickly enough to avoid missing SLAs.

3.1.2 NVM Middleware Design Overview

We design NVM Middleware with two main design goals.

Workload-aware Contention Management. The NVM Middleware leverage insights about the workload characteristics and performance requirements of applications to make informed decisions about resource allocation and contention resolution. It dynamically adjusts resource allocation for each application type independently, mitigating performance degradation caused by contention and enabling efficient resource sharing among co-located applications.. This adaptive approach enables the NVM Middleware to allocate resources judiciously to maximize overall system efficiency and meet diverse performance requirements of both interactive and batch applications. By using the workload-aware contention management offered by the NVM Middleware, a storage system using Optane PMem can effectively balance the needs of different workload types, ensuring optimal performance and fair share of resources.

RL-driven autoscaling policies. Our solution proposes the use of Reinforcement Learning to dynamically scale resources, learning from historical data and anticipating changes in workload patterns. By incorporating information from SLAs to guide the learning process, the NVM Middleware can quickly adapt to changing worload patterns over time and meet SLA objectives more effectively than traditional threshold-based approaches [47]. Moreover, given the dynamic and unpredictable nature of FaaS workloads, we propose a model-free algorithm, Q-Learning, to continuously learn the optimal policy based on

25

observed experiences, allowing the NVM Middleware to adapt to new scenarios without needing to explicitly model them.

3.2   NVM Middleware Architecture
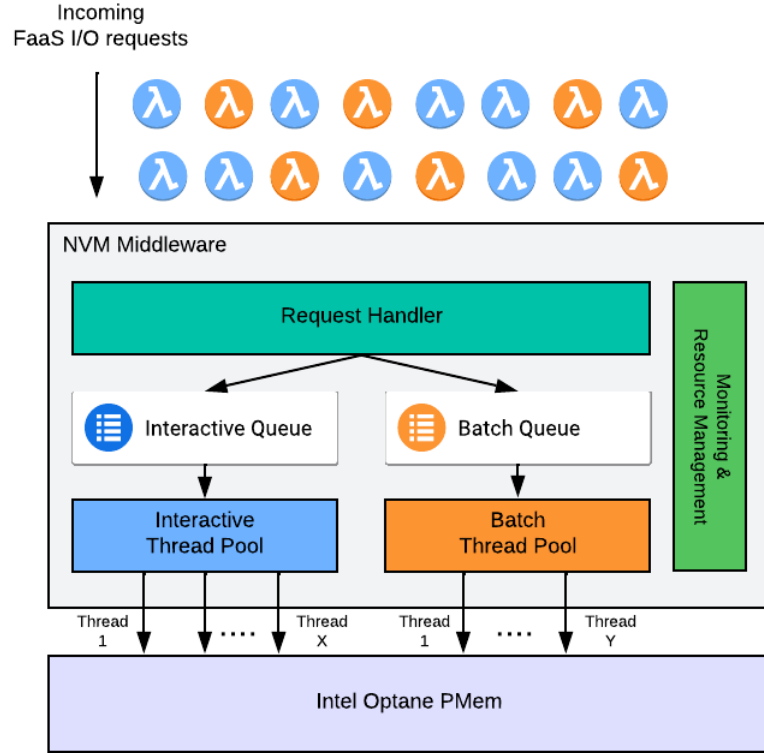
Figure 3.2: Illustration depicting the architecture of the NVM Middleware, which serves as an optimization layer for Optane PMem. The NVM Middleware governs the concurrency level on the device, categorizing incoming I/O requests based on their type (blue for interactive and orange for batch) and assigning distinct worker threads for interactive or batch workloads. The number of threads for each workload type is dynamically configurable to adapt to the system's requirements.

Figure 3.2 provides an overview of the NVM Middleware architecture. Positioned as a middle layer connecting user applications with Optane PMem, its design is tailored for

26

seamless integration within a storage service, serving as an optimization layer specifically targeting Optane PMem. It comprises a request handler, two concurrency thread pools, and a monitoring and resource management module.

The request handler serves as the primary interface for handling user I/O requests. Upon receipt, it segregates requests into two distinct non-blocking First-In-First-Out (FIFO) queues: one tailed for interactive requests and the other for batch ones. Leveraging insights into workload characteristics, the handler intelligently allocates requests to the appropriate queue. Moreover, each queue is assigned a dedicated pool of worker threads tasked with dispatching I/O requests to Optane PMem using PMEMKV. These worker threads are categorized as either interactive or batch threads. Notably, these thread pools operate independently and are dynamically managed and scaled by the Reinforcement Learning agent to meet predetermined latency and throughput goals.

The Monitoring and Resource Management module offers an interface to monitor system load and SLA performance metrics. This module initiates a separate control thread tasked with gathering data on key parameters within the NVM Middleware, such as 99th latency, throughput, and system load. Utilizing this information, the RL agent makes data-driven decisions regarding optimal thread pool scaling. Subsequently, these decisions are communicated to the Monitoring and Resource Management module, which executes the required actions within the NVM Middleware.

3.3   NVM Middleware Programming Interface

Table 3.1 outlines the NVM Middleware's programming interface, presenting a set of functions designed to facilitate interaction with a storage system and the reinforcement learning agent.

The *start* function initializes the PMEMKV database, initializes the thread pools with an initial thread count, and triggers the system monitoring within the Monitoring and Resource Management Module. In contrast, the *stop* function terminates the database connection, halts all threads in the thread pools, and stops system monitoring. Furthermore,

Table 3.1: Overview of the NVM Middleware programming interface, categorized by functionality. *System* functions facilitate resource management within the NVM Middleware, including database initialization and thread pool management. *Storage* functions provide a fundamental key-value interface for submitting requests aimed at accessing persistent memory. *RL* functions provide utilities for the reinforcement learning process, enabling monitoring of system statistics, state retrieval, and triggering scaling actions.

Category	API Name	Functionality
System	start(db, interactiveThreads, batchThreads)	Create the PMEMKV database, start thread pools, and initiate NVM Middleware's monitoring.
System	stop()	Close PMEMKV database, stop thread pools, and stop NVM Middleware's monitoring.
Storage	get(key, mode)	Submits request to retrieve a key from persistent memory.
Storage	put(key, value, mode)	Submits request to write a key to persistent memory.
RL	get_stats()	Provides the 99th percentile and throughput observed by the NVM Middleware.
RL	get_state()	Provides the current state within the NVM Middleware.
RL	perform_action(action)	Triggers a scaling action.

the *get* and *put* functions facilitate key-value interactions with the persistent memory, allowing for read and write operations. These functions are designed to accommodate hints regarding the request type (e.g., latency-sensitive or throughput-oriented), aiding the request handler in queue allocation.

The *get_stats* function furnishes insights into the 99th percentile and throughput observed by the NVM Middleware at any given moment. Similarly, the *get_state* function provides real-time state information as outlined in Table 3.2. Finally, the *perform_action* function accepts scaling actions detailed in Table 3.3 and initiates the corresponding action within the NVM Middleware.

3.4 Reinforcement Learning Component

In this section, we discuss the Q-learning algorithm used by the RL agent to dynamically adjust the number of threads assigned to each thread pool. The agent's goal is to find the best combination of threads that meets predetermined latency and throughput SLAs while minimizing contention and ensuring efficient utilization of Optane PMem.

3.4.1 Integration with the NVM Middleware
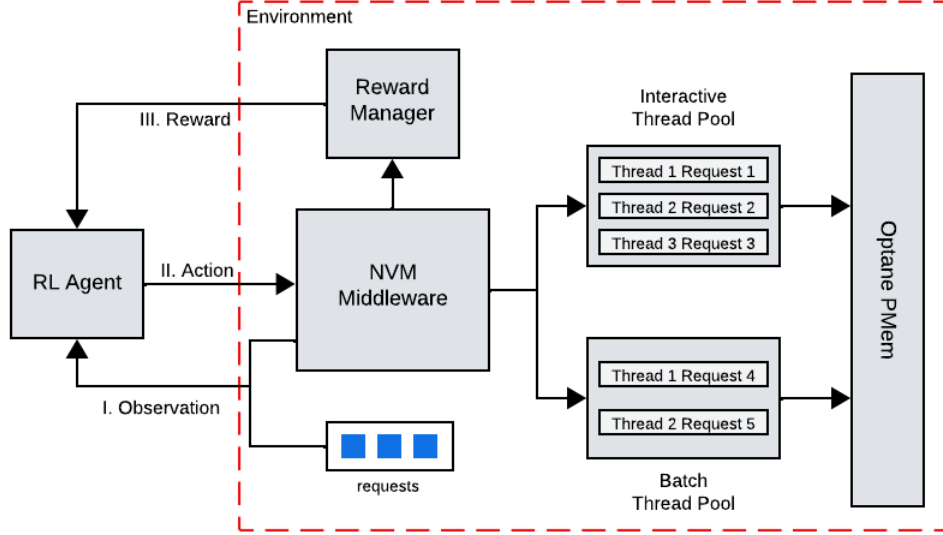
Figure 3.3: Interaction between the RL agent and the NVM Middleware. At each time step, the RL agent observes (I) the state of the environment and takes a scaling action (II) on the NVM Middleware based on its learned policy. Subsequently, the agent receives a reward (III), which is utilized to iteratively refine its policy.

Figure 3.3 offers a visual representation of the interaction between the RL agent and the NVM Middleware. At each time step, the NVM Middleware receives a diverse influx of requests, spanning both interactive and batch tasks. These requests necessitate translation into actionable I/O commands directed towards the Optane PMem.

Concurrently, the RL agent adeptly captures the environment's current state, leveraging real-time workloads' characteristics and performance metrics provided by the monitoring module. Utilizing this information, the agent orchestrates the selection of an optimal action, guiding the dynamic adjustment of threads within the interactive and batch thread pools. This adaptive decision-making process is exemplified by actions like augmenting the count of interactive threads to address evolving workload demands.

Following action selection, the NVM Middleware's resource management module implements the chosen course of action, fine-tuning the NVM Middleware's interactive and batch threads to efficiently handle incoming user requests. Upon the completion of each time step, the action's effectiveness is rigorously assessed against predefined SLA targets, yielding a reward signal generated by a reward manager.

The reward serves as invaluable feedback for the RL agent, empowering iterative policy updates aimed at refining decision-making strategies in subsequent time steps. Thus, the presented framework embodies a recursive learning cycle, wherein the RL agent continuously hones its behavior through real-world interactions, ensuring adaptive responsiveness to evolving workload dynamics.

3.4.2 Reinforcement Learning Model

State Space

Table 3.2: State representation for the reinforcement learning model. The number of interactive and batch threads is capped at 32, as measurements showed performance degradation with more than 32 threads. The interactiveQueueSize and batchQueueSize represent the number of requests in the respective queues within the NVM Middleware. The block sizes and write ratios are determined by analyzing the I/O requests received from client workloads.

Name	Description	Values
interactiveThreads	Number of interactive threads assigned to the interactive thread pool.	$1 \leq \text{interactiveThreads} \leq 32$
batchThreads	Number of batch threads assigned to the batch thread pool.	$1 \leq \text{batchThreads} \leq 32$
interactiveQueueSize	Number of requests in the interactive queue.	$\text{interactiveQueueSize} \in \mathbb{R}^+$
batchQueueSize	Number of requests in the batch queue.	$\text{batchQueueSize} \in \mathbb{R}^+$
interactiveBlockSize	Average data access size of interactive workload.	$\text{interactiveBlockSize} \in \mathbb{R}^+$
batchBlockSize	Average data access size of batch workload.	$\text{batchBlockSize} \in \mathbb{R}^+$
interactiveWriteRatio	Proportion of write requests compared to read requests in the interactive workload.	$\text{interactiveWRatio} \in \mathbb{R}^+$
batchWriteRatio	Proportion of write requests compared to read requests in the batch workload.	$\text{batchWRatio} \in \mathbb{R}^+$

Table 3.2 presents the features of our state representation. At each time step t, we define the state s_t as a tuple:

$$s_t = (\text{interactiveThreads}_t, \text{batchThreads}_t, \text{InteractiveQueueSize}_t, \text{batchQueueSize}_t,$$

$$\text{interactiveBlockSize}_t, \text{batchBlockSize}_t, \text{interactiveWRatio}_t, \text{batchWRatio}_t)$$

where $s_t \in S$ represents the state space. The tuple encapsulates the key features characterizing the system's current state, including the number of interactive and batch threads, number of pending requests in the NVM Middleware's queues, individual workload data access sizes, and write ratio for both interactive and batch workloads.

Action Space

Table 3.3: Possible actions in the action space of reinforcement learning and their effects on the NVM Middleware's concurrency control mechanism.

Action	Effect on Interactive Threads	Effect on Batch Threads
0	No change	No change
1	Increase by 1	No change
2	Decrease by 1	No change
3	No change	Increase by 1
4	No change	Decrease by 1
5	Increase by 1	Increase by 1
6	Increase by 1	Decrease by 1
7	Decrease by 1	Increase by 1
8	Decrease by 1	Decrease by 1

Table 3.3 illustrates the feasible actions within the action space. Each action corresponds to a potential adjustment in the number of interactive and batch threads. The table enumerates nine distinct actions, each with its respective effect on the number of interactive threads and batch threads.

31

Mathematically, the set of actions A is defined as $A = \{0, 1, 2, 3, 4, 5, 6, 7, 8\}$ for a given state $s_t \in S$.

Reward

To guide the optimization process of the reinforcement learning agent, we establish an algorithm (Algorithm 1) to calculate a reward value based on observed and target latency and throughput metrics. This algorithm, outlined below, serves as a crucial component in training the RL agent to make informed decisions.

1. Lines 1-5 define goals, scaling factors, and penalties. The observed and target latency (lat, lat_goal) and throughput (tp, tp_goal) metrics are scaled to a normalized range using scaling factors (max_scale_lat, max_scale_tp) and minimum scale (min_scale). This normalization process ensures that both metrics contribute proportionally to the reward calculation.

2. Lines 6-7 compare the scaled latency (lat) and throughput (tp) metrics against the scaled target values for latency (lat_goal) and throughput (tp_goal). The absolute differences between observed and target values are computed to quantify the error in latency ($error\_lat$) and throughput ($error\_tp$).

3. Lines 8-12 determine the reward based on three distinct scenarios. Firstly, if both latency and throughput goals are achieved, a high positive reward is assigned. Secondly, if both goals are not met, a low negative reward is assigned, taking into account both latency and throughput errors. The disparity in penalties, represented by $lat\_penalty$ and $tp\_penalty$, ensures that both types of errors contribute proportionately to the overall reward. Thirdly, if only the latency goal remains unmet, a low negative reward is assigned, incorporating the latency penalty and error. Finally, if only the throughput goal is unmet, a similar low negative reward is assigned, encompassing the throughput penalty and error.

32

Algorithm 1: Reward Calculation Algorithm

Input: System statistics: stat
Output: Reward value: reward
```
/* Initialize variables                                        */
```
1 max_scale_lat ← 1000, max_scale_tp ← 10, min_scale ← 1, lat_goal ← 200,
   tp_goal ← 250000, lat_penalty ← 500.0, tp_penalty ← 5000.0;
```
/* Scale observed and target latency and throughput            */
```
2 lat ← ((max_scale_lat − min_scale) × (stat.tailLatency − min_value)/(max_latency −
   min_value)) + min_scale;
3 tp ← ((max_scale_tp − min_scale) × (stat.throughput −
   min_value)/(max_throughput − min_value)) + min_scale;
4 lat_goal ← ((max_scale_lat − min_scale) × (lat_goal − min_value)/(max_latency −
   min_value)) + min_scale;
5 tp_goal ← ((max_scale_tp − min_scale) × (tp_goal − min_value)/(max_throughput −
   min_value)) + min_scale;
```
/* Calculate errors                                            */
```
6 error_lat ← |lat − lat_goal|;
7 error_tp ← |tp − tp_goal|;
```
/* Calculate reward                                            */
```
8 **if** $lat \leq lat\_goal$ **and** $tp \geq tp\_goal$ **then**
9 | reward ← 10 × (error_lat + error_tp) ;   // High reward for meeting both
        latency and throughput goals
10 **else**
11 | **if** $lat > lat\_goal$ **and** $tp < tp\_goal$ **then**
12 | | reward ← −1 × (lat_penalty × error_lat + tp_penalty × error_tp) ;
          // Penalize for high latency and low throughput
13 | **else**
14 | | **if** $lat > lat\_goal$ **then**
15 | | | reward ← −1 × lat_penalty × error_lat ; // Penalize for high latency
16 | | **else**
17 | | | reward ← −1 × tp_penalty × error_tp ;   // Penalize for low
         throughput
18 | | **end**
19 | **end**
20 **end**

3.4.3 Training Methodology

Environment Design
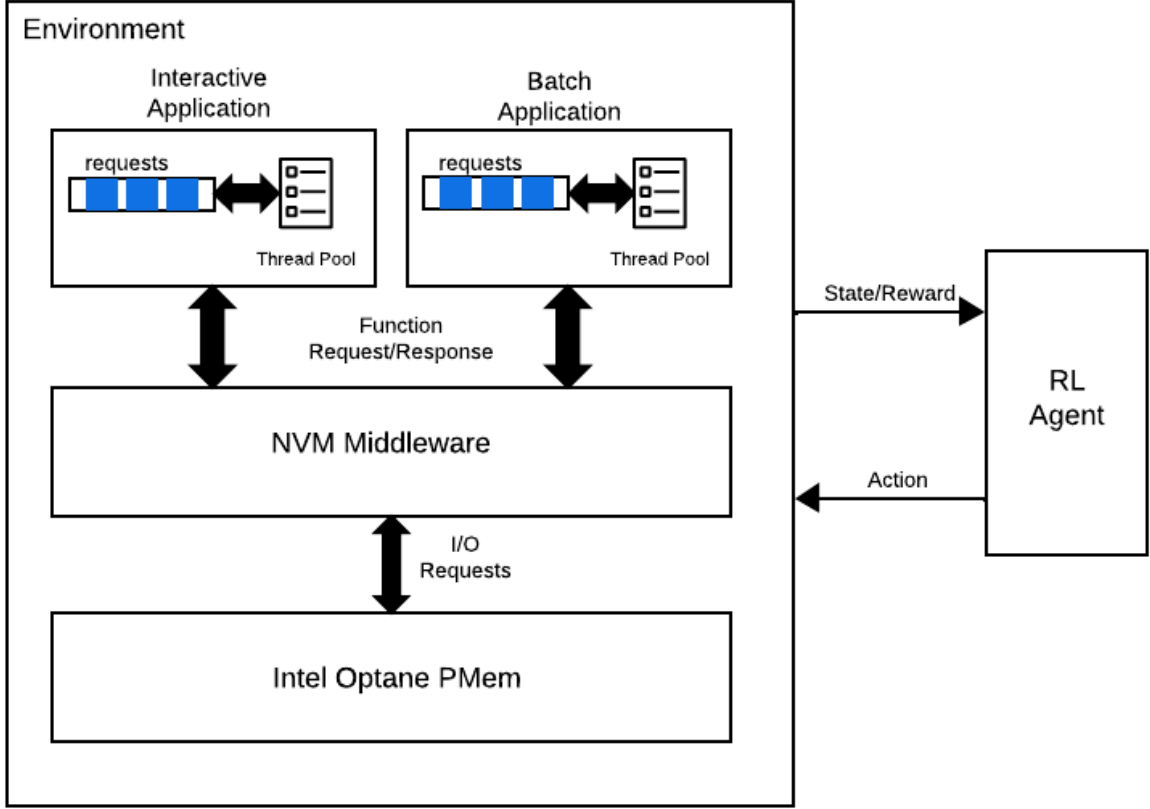
Figure 3.4: Overview of the RL environment constructed for training the RL agent. The environment employs multi-threaded interactive and batch applications to replicate workloads generated by multiple serverless functions with shared access to persistent memory. These applications interact with the NVM Middleware through function calls using its programming interface. Meanwhile, in the background, the agent continuously iterates through a closed feedback loop, observing the environment's state and executing scaling actions based on its policy.

The environment architecture designed for training and evaluating the RL agent is depicted in Figure 3.4. This architecture comprises several key components, including an interactive multi-threaded application, a batch multi-threaded application, the NVM Middleware, and Intel Optane PMem.

To simulate a multi-tenant serverless scenario, both applications are executed concurrently. Workload patterns for each application are derived from collected serverless traces. To emulate high concurrency levels typical in serverless environments, multiple threads within each application are employed to dispatch requests to the NVM Middleware via the API described in Section 3.3. Meanwhile, the NVM Middleware processes these requests in accordance with the workflow outlined in Section 3.2.
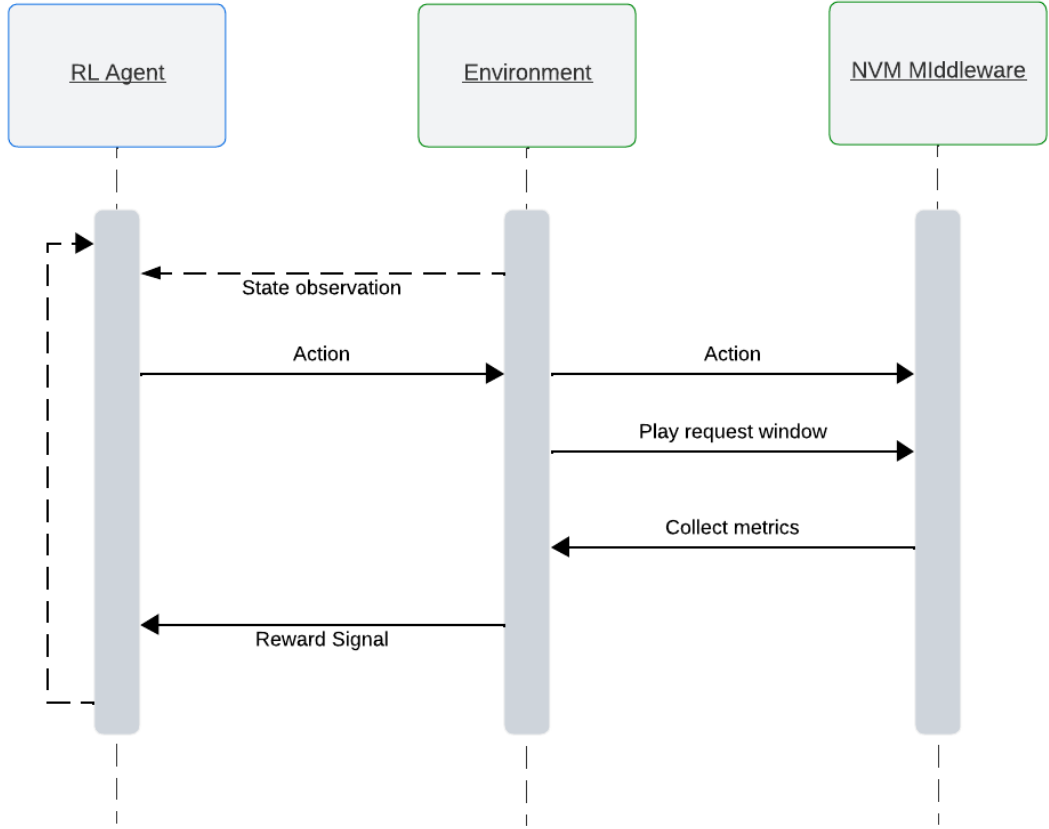
Figure 3.5: Illustration depicting the interaction between the RL agent and its environment at each time step. During each time step, the agent executes a scaling action, followed by the processing of the subsequent window of I/O requests by the environment. Subsequently, the environment gathers latency and throughput metrics to assess the effectiveness of the action, providing a reward signal that the agent utilizes to refine its policy.

In order to model the time steps inherent in an RL process, the environment organizes the applications' requests into 1-second windows, processing one window per time step. Figure 3.5 illustrates the interactions between the RL agent and the environment at each time step. Beginning with a state observation from the preceding step, the agent communicates the intended action to the environment. Subsequently, the environment relays this action to the NVM Middleware, which then allocates resources accordingly. Upon successful execution of the action, the environment initiates processing for the next window of requests. Once all requests within the window are handled, the environment gathers metrics from the NVM Middleware and furnishes a new state observation along with a reward signal to the agent. The agent utilizes this reward to update its policy, perpetuating the iterative learning process.

Function Approximation

To address the challenge posed by the continuous state space in our environment, traditional Q-learning approaches become impractical due to the vast number of states that cannot be feasibly mapped into a Q-table. Consequently, we employ function approximation techniques to estimate the value of each action based on the state.

Specifically, we train nine separate regression models, each corresponding to one of the available actions, using stochastic gradient descent. This approach allows us to capture the underlying patterns in the data and generalize across states not encountered during training, enabling our agent to make informed decisions even in novel situations.

However, selecting appropriate hyperparameters for our regression models presents a significant challenge. Online training alone is insufficient for accurately assessing model performance, as it can be time-consuming and computationally intensive. To overcome this limitation, we adopt a batch learning approach with offline historical data.

By leveraging historical data collected from the environment, we can tune our models' hyperparameters and incorporate prior knowledge into our RL agent. This approach accelerates the learning process by bootstrapping our models with valuable insights gained from past experiences [47, 48].

To construct our dataset, we deploy a non-optimal agent that performs random actions in the environment, capturing state-action-reward transitions. Following established machine learning practices, we split the dataset into training and testing sets and employ 5-fold cross-validation on the training set to evaluate model performance rigorously.

Additionally, we preprocess the features by standardizing them using the standard scaler and apply polynomial preprocessing to enhance the model's ability to capture non-linear relationships within the data.

Proposed Q-Learning Algorithm

Algorithm 2 outlines the Q-Learning process for training an agent to make optimal decisions in the environment. It takes the bootstrapped Q-value models M_a for all actions a and outputs the new learned models after training.

The algorithm initializes the training parameters and then iterates over a specified number of episodes. Within each episode, the environment is reset, and the agent interacts with it until the episode is complete. At each step, the agent observes the current state s_t, selects an action a_t based on an ϵ-greedy policy, takes the action, and observes the resulting reward r and next state s_{t+1}.

The Q-value models are updated based on the observed reward and next state. If the episode is not done, the target Q-value is calculated using the reward and the maximum Q-value for the next state. If the episode is done, the target Q-value is simply set to the reward.

The model for the selected action a_t is updated using the target Q-value, and the state is updated to the next state. Additionally, the exploration rate ϵ is decreased according to an exploration schedule.

Algorithm 2: Q-Learning Algorithm

Input: Pre-trained Q-value models M_a for all actions a
Output: Learned Q-value models M_a for all actions a

1 Initialize the training parameters α, γ, ϵ;

2 for $episode \leftarrow 1$ **to** E **do**

3   Reset the environment;

4   **repeat**

5   Observe the state s_t;

         `// Choose action` a_t `using the` ϵ`-greedy policy`

6   Generate random number r from uniform distribution in $[0, 1]$;

7   **if** $r < \epsilon$ **then**

8   Select a random action a_t from the action space ;

9   **end**

10   **else**

11   **for** *each action a* **do**

12   Predict Q-value $Q_a(s_t)$ using model M_a: $Q_a(s_t) \leftarrow M_a.predict(s_t)$;

13   **end**

14   Select action $a_t \leftarrow \arg\max_a Q_a(s_t)$;

15   **end**

16   Take action a_t, observe reward r and next state s_{t+1};

         `// Update the Q-value model using reward and next state`

17   **if** *not done* **then**

18   **for** *each action a* **do**

19   Predict Q-value $Q_a(s_{t+1})$ using model M_a:
                 $Q_a(s_{t+1}) \leftarrow M_a.predict(s_{t+1})$;

20   **end**

21   Calculate target Q-value: $target \leftarrow r + \gamma \cdot \max_a Q_a(s_{t+1})$;

22   **end**

23   **else**

24   Set target Q-value to the reward: $target \leftarrow r$;

25   **end**

26   Update the model for action a_t with the target Q-value:
         $M_{a_t}.partial\_fit(s_t, target)$;

27   Update state: $s_t \leftarrow s_{t+1}$;

28   **until** *episode is done*;

29   Decrease ϵ according to exploration schedule;

30 end

3.5 Implementation

The NVM Middleware, detailed in Section 3.3, is implemented using C++. We leverage PMEMKV from the Persistent Memory Development Kit [15] to facilitate reading and writing data into Intel Optane PMM. To manage concurrent operations efficiently, we utilize the non-locking, concurrent queue provided by the Intel Threading Building Blocks [49] library for both the interactive and batch queues.

For the RL Environment, as described in Section 3.4.3, we adopt a hybrid approach employing C++ and Python. The environment itself is constructed in C++, aligning with the specifications outlined in Section 3.4.3. Conversely, the RL agent and the Q-Learning algorithm, also discussed in the same section, are developed using Python. We leverage the SGDRegressor model from the Scikit-learn[50] library to facilitate the representation of our regression models for function approximation. Additionally, we employ Scikit-learn for hyperparameter tuning. To seamlessly integrate the C++ and Python components, we utilize pybind11[51].

Chapter 4: Evaluation

This chapter provides an evaluation of the NVM Middleware. Firstly, we describe the experimental setup utilized for our evaluations. Next, we assess the performance advantages derived from the concurrency control mechanism integrated into the NVM Middleware. Finally, we evaluate the effectiveness of our reinforcement learning model and Q-Learning algorithm. Specifically, we train an agent and subsequently assess its capacity to adhere to predefined service level agreements amidst dynamic workload variations.

4.1 Experimental Setup

4.1.1 Platform

Table 4.1: Experimental Platform Specifications

Processor	Intel® Xeon® Gold 6252
Sockets	2
Cores per socket	24
Threads per core	2
Numa nodes	2
CPU Frequency	2.7 GHz (3.7 GHz Turbo frequency)
L1d cache	1.5 MiB
L1i cache	1.5 MiB
L2 Cache	48 MiB
L3 Cache	71.5 MiB
DRAM	16 GB DDR4 DIMM x 6 per socket
Persistent Memory	128 GB Optane PMem DIMMs x 6 per socket
Operating System	Ubuntu 20.04.4 LTS (Focal Fossa)

The experimental platform utilized in this study is detailed in Table 4.1.1. It features an Intel® Xeon® Gold 6252 processor with 2 sockets, each hosting 24 cores and 2 threads

per core, totaling 2 NUMA nodes. Each socket is equipped with three memory channels, housing 16 GB DDR4 DIMMs and 128 GB Optane PMem DIMMs. In aggregate, the system comprises 192 GB of DRAM and 1.5 TB of persistent memory. To mitigate the NUMA effect, one socket is designated for running the NVM Middleware threads, while the other handles the interactive and batch applications, as described in Section 3.4.3.

4.1.2 Optane PMem Configuration

As outlined earlier, this thesis concentrates on exploring the persistent capabilities of Optane PMem. Consequently, Optane PMem is employed in the App Direct Mode throughout our experiments. To facilitate the utilization of persistent memory, we expose it via an xfs filesystem configured in dax mode, thereby bypassing the page cache. Additionally, we enhance memory management and performance by configuring the persistent memory with huge pages (2MiB) [20]. Lastly, we deploy a PMEMKV database with a capacity of 600GB, configured with its persistent concurrent engine.

4.1.3 Workload Generators

We deploy the interactive and batch applications outlined in Section 3.4.3 utilizing two distinct workload generators.

Yahoo! Cloud Serving Benchmark (YCSB)

YCSB [52] is a multi-threaded benchmark specifically tailored for assessing cloud-based databases and storage systems. Utilizing YCSB, we emulate interactive applications by generating small byte requests. To vary the workload characteristics, we modify parameters such as the read-to-write ratio, request distribution, and client threads. Leveraging the C++ version of YCSB, we extend its functionality to facilitate API calls to the NVM Middleware.

Serverless Trace Replay

We develop the Serverless Trace Replay tool in-house to replicate workloads typically encountered in real-world serverless environments. This tool operates by reading a file containing workload traces and executing them accordingly. To simulate multiple serverless functions, the tool spawns multiple threads to issue requests concurrently.

For emulating an interactive application, we utilize traces collected from Azure Functions, sourced from a dataset available in [53]. This dataset (described in more detail in [23]) offers a comprehensive log of Azure Function blob accesses over HTTPS recorded between November and December 2020. Specifically, our experiments utilize requests recorded on December 6, 2020, with a specific emphasis on those involving small data access sizes (less than 1 KB), which typically signify interactive application behavior.

For modeling a batch application, we collect traces from Wukong, a serverless parallel computing framework [4]. The traces are acquired by executing a Single Value Decomposition job for a $128kx128k$ matrix on Wukong and capturing the resulting I/O requests generated by the framework. This dataset offers a precise representation of throughput-oriented serverless data-analytics applications, characterized by significant parallelism and substantial data access sizes spanning from 4KB to 200MB.

4.2 Efficiency of the Workload-Aware Concurrency Control Mechanism

We evaluate the effectiveness of the workload-aware concurrency control mechanism embedded within the NVM Middleware compared to a baseline scenario devoid of concurrency control. In the baseline setting, concurrency control is inactive, permitting a maximum of 200 concurrent data accesses on Optane PMem. This assessment involves deactivating the reinforcement learning agent and system monitoring, with a primary focus on the 99th percentile latency and throughput observed by client applications.

Six experiments are conducted, running concurrently YCSB and the Serverless Trace Replay simulating SVD traces. Each YCSB experiment varies parameters such as data access size (64B, 128B), read-to-write ratio (50-50, 100-0), and data request distribution (zipfian, uniform), while the Serverless Trace Replay maintains consistent settings across experiments. Both applications are executed with 100 client threads.

In each experiment, the baseline scenario is executed without concurrency control, followed by 42 additional tests exploring various combinations of interactive and batch threads within the NVM Middleware. Each run maintains a fixed combination of interactive (I) and batch (B) threads. Subsequently, the 99th percentile latency observed by YCSB requests and the overall throughput reported by the Serverless Trace Replay are recorded. The results are depicted in Figures 4.1, 4.2, and 4.3.

Our observations indicate substantial benefits from the concurrency control implemented by the NVM Middleware across most scenarios. Relative to the baseline, the NVM Middleware demonstrates potential enhancements, including up to a $435x$ decrease in the tail 99th percentile latency and an $8x$ increase in throughput.. Notably, certain thread combinations achieve sub-millisecond access latencies with a more predictable behavior, significantly improving application performance. However, improper thread configuration within the NVM Middleware, either insufficient or excessive, results in performance degradation exceeding that of the baseline. This emphasizes the criticality of meticulously selecting the optimal thread combination, as an incorrect choice may yield similar or inferior results compared to operating without concurrency control.

A key query arising from these findings concerns determining the optimal thread combination. We observe that prioritizing interactive threads yields sub-millisecond access latencies but compromises peak throughput. Conversely, increasing batch threads to enhance throughput metrics leads to higher access latencies. Addressing this dilemma entails selecting a combination of interactive and batch threads that satisfies both latency and throughput SLA metrics, a topic elaborated upon in the subsequent section.

Figure 4.1: Evaluation of the NVM Middleware's concurrency control mechanism when co-running SVD I/O traces (batch) and a YCSB workload (interactive) configured with zipfian request distribution and an even distribution of read and write requests. Two runs are performed configuring YCSB with 64B and 128B data access sizes. Both applications utilize 100 client threads to send requests to the NVM Middleware. The illustration presents statistics on throughput (yellow line) and 99th percentile latency (green box plot) obtained under different configurations of the NVM Middleware, denoted as I/B (Interactive threads/Batch threads). These statistics are compared against a baseline scenario with no concurrency control (blue line and blue box plot). The latencies observed by YCSB are depicted as a distribution, ranging from the minimum to the maximum observed, along with quartiles and median values.

Figure 4.2: Evaluation of the NVM Middleware's concurrency control mechanism when co-running SVD I/O traces and a pure read YCSB workload with Zipfian request distribution. Two runs are performed configuring YCSB with 64B and 128B data access sizes. Both applications utilize 100 client threads to send requests to the NVM Middleware. The illustration presents statistics on throughput (yellow line) and 99th percentile latency (green box plot) obtained under different configurations of the NVM Middleware, denoted as I/B (Interactive threads/Batch threads). These statistics are compared against a baseline scenario with no concurrency control (blue line and blue box plot). The latencies observed by YCSB are depicted as a distribution, ranging from the minimum to the maximum observed, along with quartiles and median values.
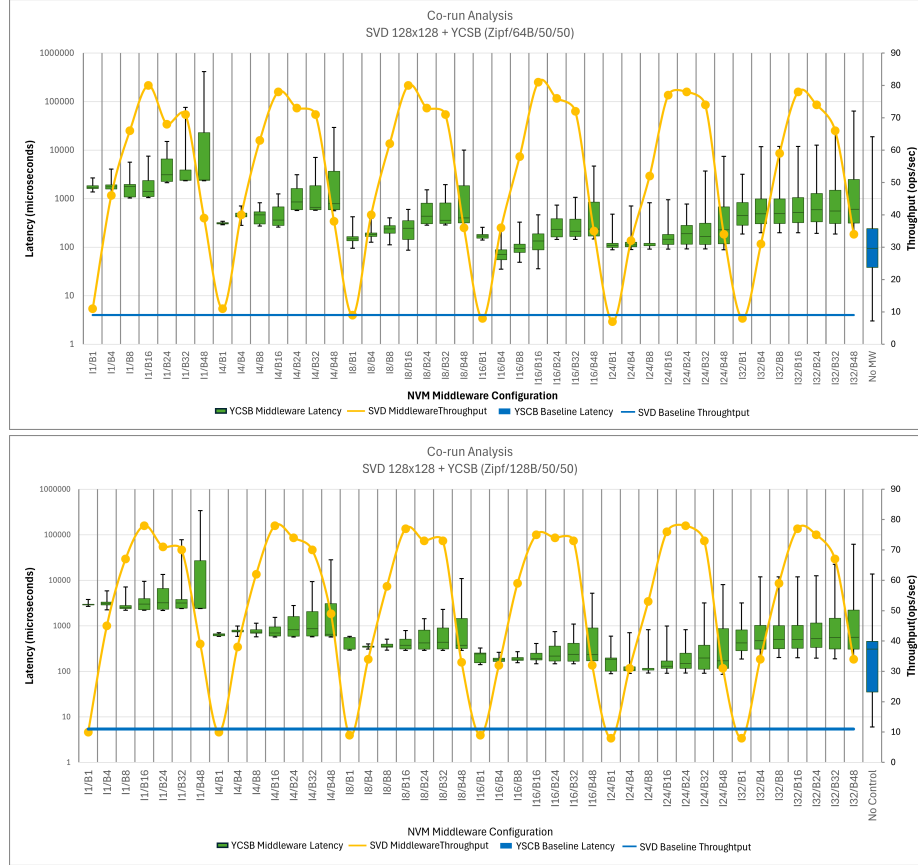
Figure 4.3: Evaluation of the NVM Middleware's concurrency control mechanism when co-running SVD I/O traces and a YCSB workload configured with uniform request distribution and an even distribution of read and write requests. Two runs are performed configuring YCSB with 64B and 128B data access sizes. Both applications utilize 100 client threads to send requests to the NVM Middleware. The illustration presents statistics on throughput (yellow line) and 99th percentile latency (green box plot) obtained under different configurations of the NVM Middleware, denoted as I/B (Interactive threads/Batch threads). These statistics are compared against a baseline scenario with no concurrency control (blue line and blue box plot). The latencies observed by YCSB are depicted as a distribution, ranging from the minimum to the maximum observed, along with quartiles and median values.
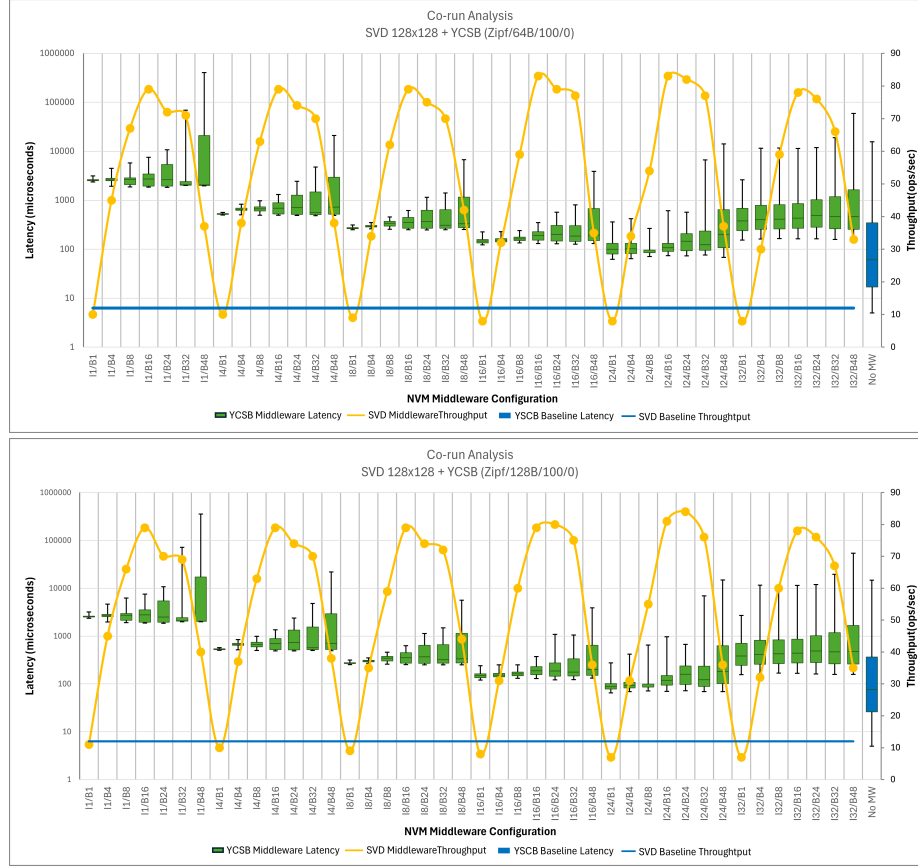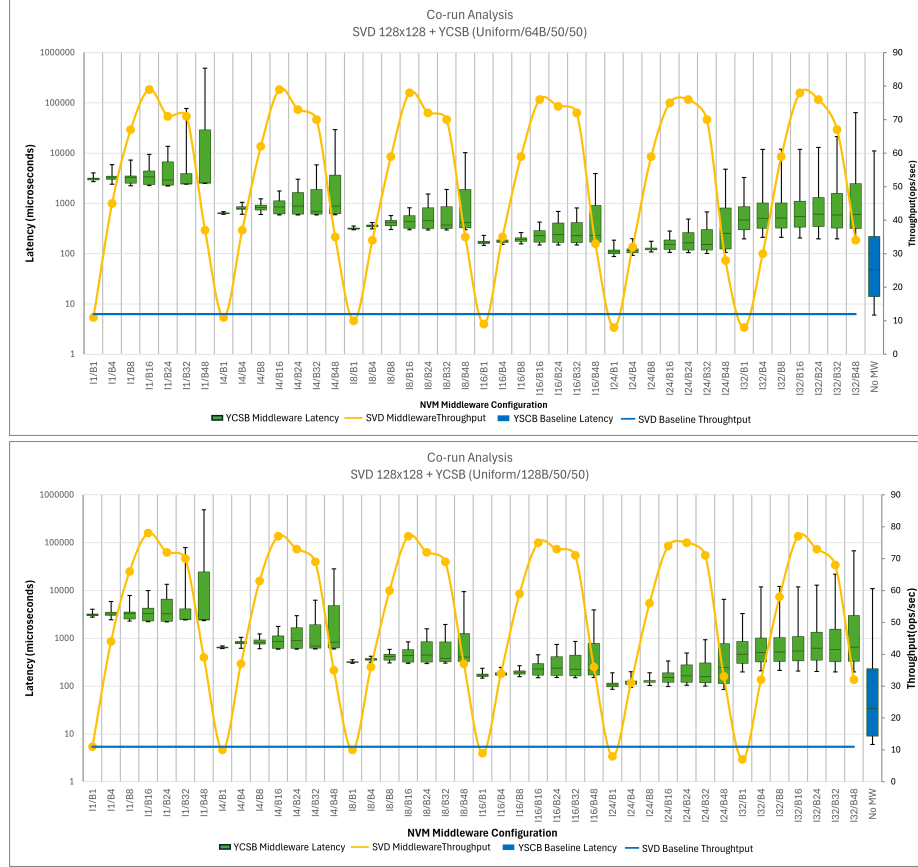
46

4.3 Meeting SLA performance using Reinforcement Learning

We present an evaluation of RL-driven policies aimed at balancing the number of interactive and batch threads to meet latency and throughput SLAs within the NVM Middleware. This experiment assesses the NVM Middleware's ability to achieve predefined SLA objectives amidst varying workloads. To this end, we construct four distinct phases, each comprising a interactive and batch application executed concurrently in the environment. Utilizing the Q-Learning algorithm (outlined in Algorithm 2), we train the RL agent to determine the optimal combination of interactive and batch threads that maximizes performance while meeting predefined latency and throughput SLA objectives for each phase. We then evaluate the agent's ability to predict and adapt to workload changes in an unknown environment where phases are randomly alternated.

Workload Phases

To evaluate the learning capabilities of the RL agent in adapting thread combinations for optimal performance and meeting predefined SLA metrics, we design four distinct phases. Leveraging I/O traces collected from Azure Functions and Wukong, we construct interactive and batch workloads by adjusting parameters such as data access size, read-to-write ratio, and client threads for each application. We intensify the workload by accelerating the pace of the traces and loop the execution to ensure sufficient simulation steps.

The phases are structured as follows:

Phase 1: We utilize 2039 requests from Azure Function blob access traces captured on December 6, 2020, between 8:20 PM and 8:22 PM. These requests are primarily reads, with a read-to-write ratio of 80-20 and data access sizes ranging between 30B and 50B. For the batch workload, we employ a subset of SVD traces comprising 3847 requests, maintaining a 50-50 read-to-write ratio and a fixed data access size of 800KB. Both applications are configured with 200 client threads for concurrent request handling.

Phase 2: The interactive workload remains unchanged from Phase 1, while the number of client threads is reduced to 150. Similarly, the batch workload maintains its configuration but with an increased number of concurrent client threads set to 320.

Phase 3: The interactive workload is consistent with Phase 1, but with an escalation in client threads to 400. For the batch workload, we modify the SVD traces to employ a fixed data access size of 4k and transition to a read-only workload. Concurrently, we assign 200 client threads for the batch workload.

Phase 4: Drawing from Azure Function blob access traces, we incorporate 7814 requests occurring on December 6, 2020, between 1:21 PM and 1:27 PM for the interactive workload. These requests are predominantly writes, with a read-to-write ratio of 10-90 and larger data access sizes averaging around 500B. The batch workload configuration remains consistent with Phase 3. Each application is allocated 200 client threads for concurrent request processing.

Training the RL Agent

We commence the learning process by conducting model selection and hyperparameter tuning on the nine regression models employed by the RL agent (refer to Table 4.2 for tuning options). This entails generating a dataset of transitions in the environment by executing a non-optimal random agent on the environment for 150 episodes of each workload. Subsequently, we utilize these transitions to select the appropriate model and tune hyperparameters for each action. The resulting regression models are summarized in Table 4.3.

With the tuned regression models, we proceed to execute the Q-learning algorithm for each workload using the parameters detailed in Table 4.4. To address the exploration-exploitation dilemma, we initialize the epsilon value to 1 and decay it after each episode. This strategy facilitates comprehensive exploration of the state space early in training, followed by exploitation of acquired knowledge. We note that different phases require varying numbers of training episodes to converge to an optimal pattern, likely due to the

initial dataset's generation with a non-optimal policy. Initially, we conduct empirical tests (Tables 4.5 - 4.8) by fixing the NVM Middleware threads to manually ascertain the optimal combination. Subsequently, we execute Q-learning and analyze the last three episodes of each phase to determine the convergent combination of threads.

Our observations (Figures 4.4 - 4.7) indicate that the RL agent is capable of learning the optimal combination of interactive and batch threads for each workload. The learned combination of threads matches our empirical results across all workloads. For Workload A, the agent converges to utilizing approximately 10 interactive and batch threads each. Similarly, for Workload B, the agent converges to approximately 10 interactive and batch threads. For Workload C, the agent converges to approximately 7 interactive and 3 batch threads, while for Workload D, it converges to approximately 15 interactive threads and 5 batch threads.

Table 4.2: Overview of hyperparameters used in the tuning process for polynomial regression models employed in function approximation. The *degree* parameter denotes the degree of the polynomial function utilized. The *loss* parameter specifies the loss function employed during stochastic gradient descent. The *penalty* parameter represents the regularization technique applied to mitigate overfitting. The *alpha* parameter indicates the strength of the regularization penalty. The *learning_rate* parameter determines the scheduling of the model's learning rate. Finally, the *max_iterations* parameter sets the maximum number of passes over the training data.

Parameter	Values
degree	1,2,3
loss	squared, huber, epsilon_insensitive
penalty	l1, l2, elasticnet
alpha	0.1, 0.01, 0.001, 0.0001
learning rate	constant, optimal, invscaling
max_iterations	100, 1000, 10000, 100000

Table 4.3: Hyperparameters of the polynomial regression models after hyperparameter tuning.

Model	Parameters
Model_1	degree: 2, learning_rate: 'invscaling', loss: 'squared_loss', alpha: 0.1, max_iter: 1000, penalty: elasticnet
Model_2	degree: 2, learning_rate: 'invscaling', loss: 'squared_loss', alpha: 0.01, max_iter: 10000, penalty: l1
Model_3	degree: 2, learning_rate: 'invscaling', loss: 'squared_loss', alpha: 0.0001, max_iter: 100, penalty: elasticnet
Model_4	degree: 2, learning_rate: 'invscaling', loss: 'squared_loss', alpha: 0.001, max_iter: 10000, penalty: l1
Model_5	degree: 2, learning_rate: 'invscaling', loss: 'squared_loss', alpha: 0.01, max_iter: 10000, penalty: elasticnet
Model_6	degree: 2, learning_rate: 'invscaling', loss: 'squared_loss', alpha: 0.01, max_iter: 1000, penalty: elasticnet
Model_7	degree: 2, learning_rate: 'invscaling', loss: 'squared_loss', alpha: 0.01, max_iter: 1000, penalty: elasticnet
Model_8	degree: 2, learning_rate: 'invscaling', loss: 'squared_loss', alpha: 0.1, max_iter: 10000, penalty: l1
Model_9	degree: 2, learning_rate: 'invscaling', loss: 'squared_loss', alpha: 0.01, max_iter: 100, penalty: elasticnet

Table 4.4: Parameters utilized for Q-Learning by the RL agent. The target 99th percentile latency and throughput represent predefined SLAs guiding the reward calculation. The aim is to maintain the observed 99th percentile latency below 250 microseconds while ensuring throughput remains above 250,000 operations per second. The exploration rate (*epsilon*) diminishes gradually between episodes, following a decay rate (*epsilon_decay*), to strike a balance between exploration and exploitation of knowledge. Furthermores, additional episodes beyond the initially specified count are introduced to enable the agent to reach the optimal policy for phases 1, 3, and 4.

Parameter	Value
episodes	Phases $1, 3, 4$: 1,000, Phase 2: 700
steps per episode	200
gamma	0.95
learning rate	0.7
epsilon	0.9
epsilon_decay	0.1
Target 99th Latency	≤ 250 microseconds
Target throughput	$\geq 250,000$ operations/second

Table 4.5: Experimental reward analysis conducted on Phase 1 using the NVM Middleware with various fixed combinations of interactive (I) and batch (B) threads. The table displays statistics on rewards obtained under different configurations, denoted as I5/B5, I10/B10, I15/B15, I15/B5, and I5/B15. The values represent the distribution of rewards, ranging from the minimum to the maximum observed, along with quartiles and median scores. Based on these preliminary findings, the configuration with 10 interactive threads and 10 batch threads appears to yield the most favorable results for Phase 1.

	I5/B5	I10/B10	I15/B15	I15/B5	I5/B15
Min	-5,716	-8,312	-41,660	-5,682	-9,436
Q1	-1,383	2.7	-4,797	-2,971	-1
Median	-171	3.92	-2	-1,850	0
Q3	0	4.3	3	-1,035	1
Max	1	5	5	3	2

Table 4.6: Experimental reward analysis conducted on Phase 2 using the NVM Middleware with various fixed combinations of interactive (I) and batch (B) threads. The table displays statistics on rewards obtained under different configurations, denoted as I5/B5, I10/B10, I15/B15, I15/B5, and I5/B15. The values represent the distribution of rewards, ranging from the minimum to the maximum observed, along with quartiles and median scores. Based on these preliminary findings, the configuration with 10 interactive threads and 10 batch threads appears to yield the most favorable results for Phase 2.

	I5/B5	I10/B10	I15/B15	I15/B5	I5/B15
Min	-4,320	-7,763	-20,455	-5,328	-10,060
Q1	-463	-1.9	-1,169	-368	1
Median	1.3	5.2	4.2	3.1	3
Q3	1.8	5.8	4.9	3.3	4
Max	2.8	6	6	3.8	6

Table 4.7: Experimental reward analysis conducted on Phase 3 using the NVM Middleware with various fixed combinations of interactive (I) and batch (B) threads. The table displays statistics on rewards obtained under different configurations, denoted as I5/B5, I7/B3, I7/B7, I10/B10, I15/B15, I15/B5, and I5/B15. The values represent the distribution of rewards, ranging from the minimum to the maximum observed, along with quartiles and median scores. Based on these preliminary findings, the configuration with 7 interactive threads and 3 batch threads appears to yield the most favorable results for Phase 3.

	I5/B5	I7/B3	I7/B7	I10/B10	I15/B15	I15/B5	I5/B15
Min	-12,490	-6,582	-174,852	-141,354	-149,647	-96,900	-13,211
Q1	-1,230	-1,727	-2,567	-18,768	-42,951	-58,414	-8,583
Median	-272	-672	-4	-566	-14,008	-2,954	-4,940
Q3	-5	-3	-2	-1	-4,607	0	-2,709
Max	-3	-1	0	3	-1	4	-943

Table 4.8: Experimental reward analysis conducted on Phase 4 using the NVM Middleware with various fixed combinations of interactive (I) and batch (B) threads. The table displays statistics on rewards obtained under different configurations, denoted as I5/B5, I10/B10, I15/B15, and I15/B5. The values represent the distribution of rewards, ranging from the minimum to the maximum observed, along with quartiles and median scores. Based on these preliminary findings, the configuration with 15 interactive threads and 5 batch threads appears to yield the most favorable results for Phase 4.

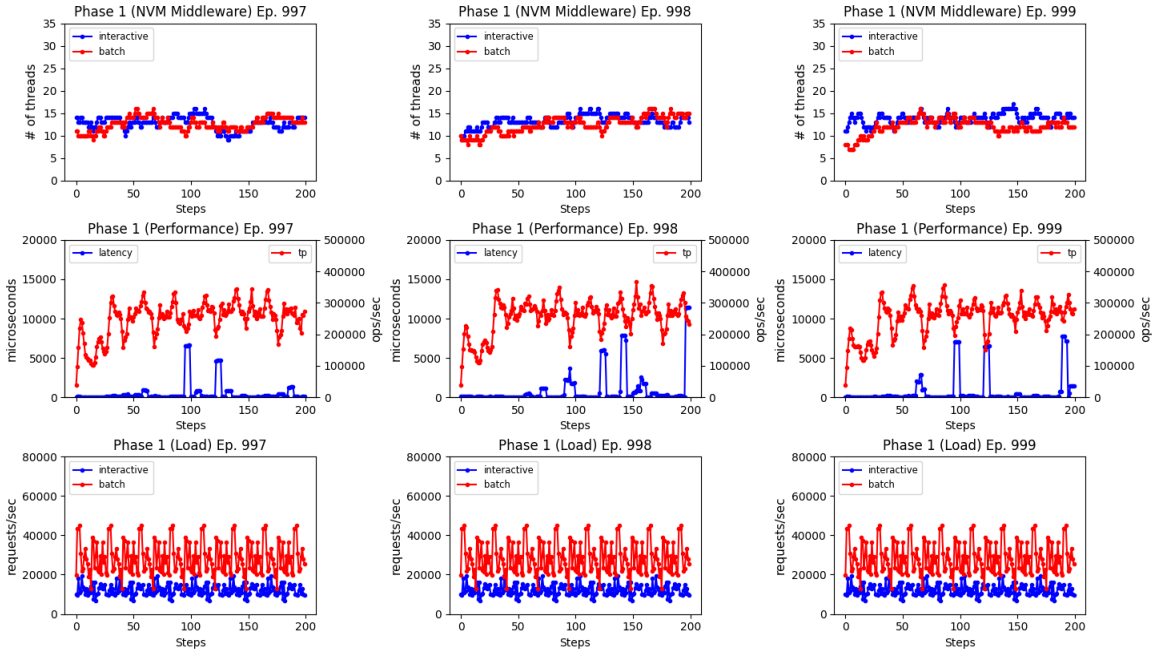|	I5/B5	I10/B10	I15/B15	I15/B5
Min	-11,341	-14,699	-21,259	-3,912
Q1	-153	-2.5	-6,908	-1
Median	-2	2.3	-3,117	3
Q3	0	3.7	-4	4
Max	3	5	3	5

Figure 4.4: Visualization depicting the learned pattern of the agent during Phase 1 of the training process. The analysis focuses on the behavior observed in the final three episodes of the Q-Learning process, which spanned 1,000 episodes. During these episodes, the exploration rate is so low that the agent predominantly exploits its accumulated knowledge. The first row illustrates the agent's configuration of the NVM Middleware with approximately 10 interactive and 10 batch threads, aligning with preliminary results for Phase 1. In the middle row, the throughput and 99th percentile latency reported by the NVM Middleware at each time step are depicted. By employing the optimal combination of threads, the agent consistently maintains low latency (less than 250 microseconds) and a throughput exceeding 250,000 operations/second across most steps. Finally, the bottom row illustrates the operations per second sent to the NVM Middleware by Phase 1.
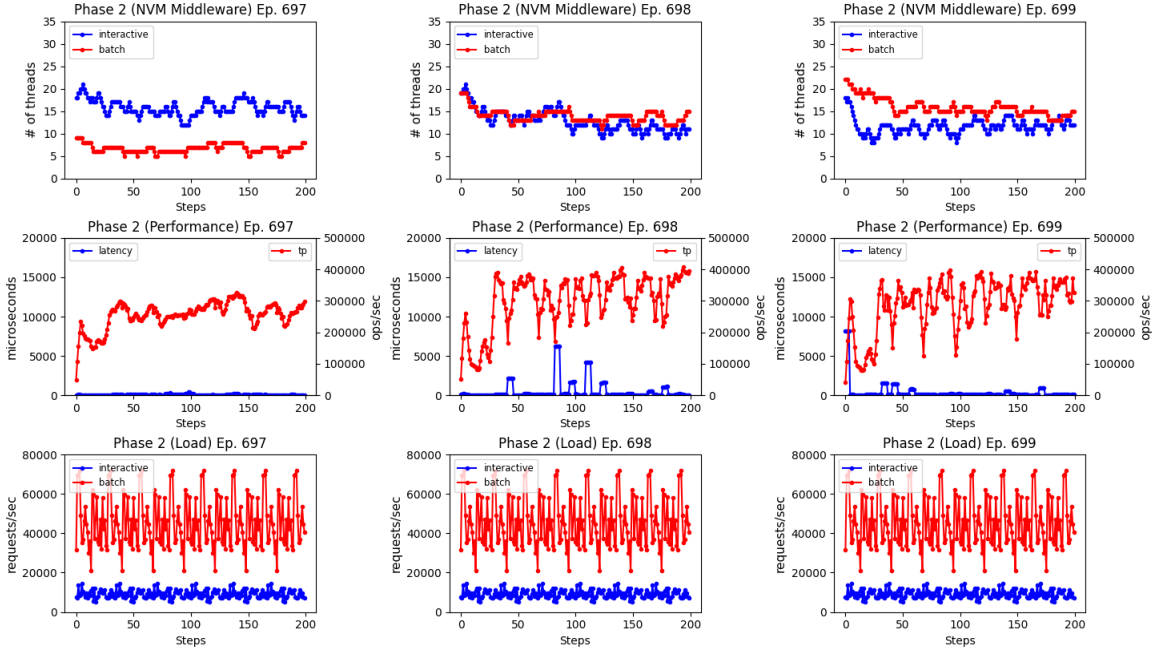
Figure 4.5: Visualization depicting the learned pattern of the agent during Phase 2 of the training process. The analysis focuses on the behavior observed in the final three episodes of the Q-Learning process, which spanned 700 episodes. During these episodes, the exploration rate is so low that the agent predominantly exploits its accumulated knowledge. The first row illustrates the agent's configuration of the NVM Middleware with high number of interactive and batch threads (between 10-15), aligning with preliminary results for Phase 2. In the middle row, the throughput and 99th percentile latency reported by the NVM Middleware at each time step are depicted. By employing the optimal combination of threads, the agent consistently maintains low latency (less than 250 microseconds) and a throughput exceeding 250,000 operations/second across most steps. Finally, the bottom row illustrates the operations per second sent to the NVM Middleware by Phase 2.
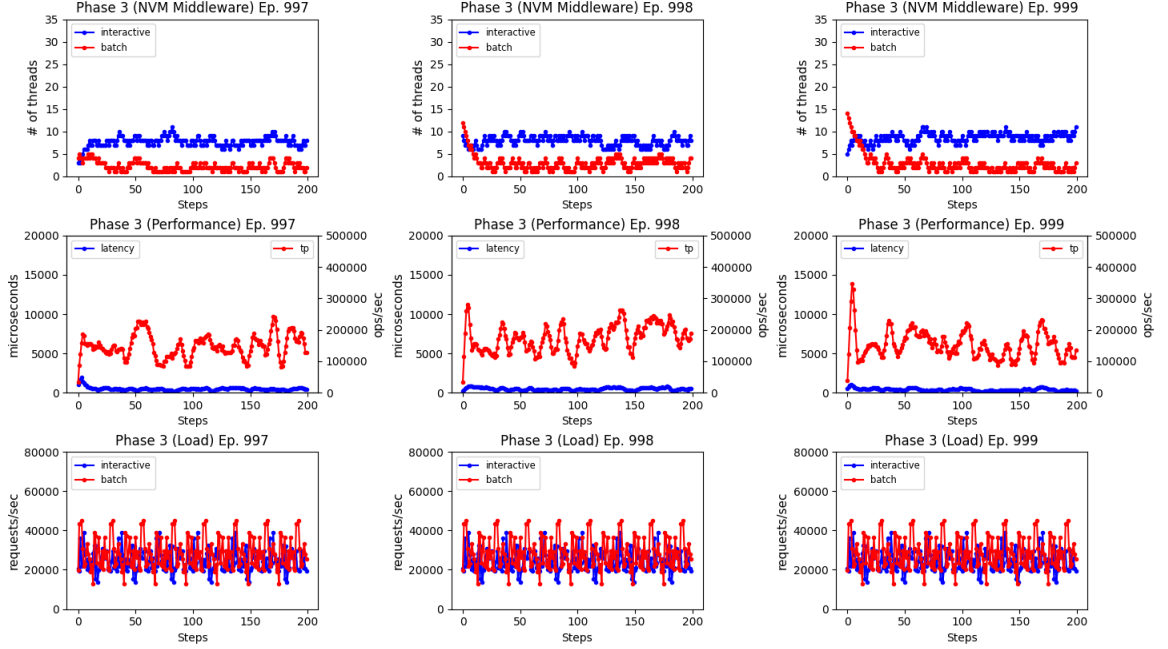
Figure 4.6: Visualization depicting the learned pattern of the agent during Phase 1 of the training process. The analysis focuses on the behavior observed in the final three episodes of the Q-Learning process, which spanned 1,000 episodes. During these episodes, the exploration rate is so low that the agent predominantly exploits its accumulated knowledge. The first row illustrates the agent's configuration of the NVM Middleware with approximately 8 interactive and low number of batch threads (approximately less than 5), aligning with preliminary results for Phase 3. In the middle row, the throughput and 99th percentile latency reported by the NVM Middleware at each time step are depicted. By employing the optimal combination of threads, the agent consistently maintains low latency (less than 250 microseconds) and a throughput exceeding 250,000 operations/second across most steps. Finally, the bottom row illustrates the operations per second sent to the NVM Middleware by Phase 3.
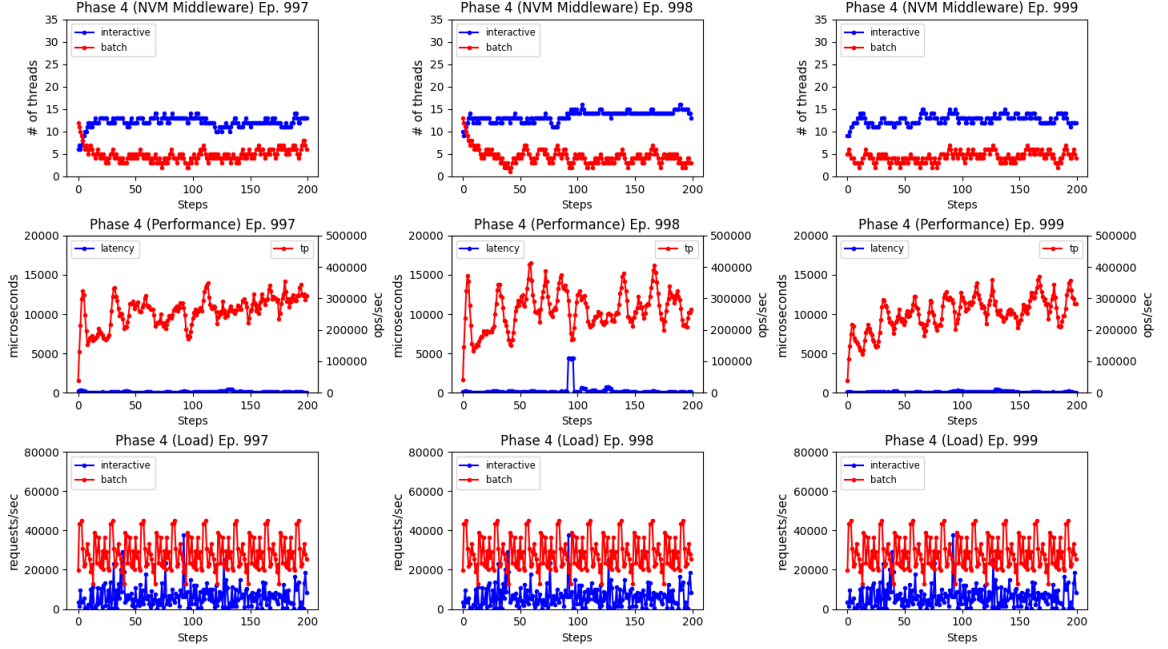
Figure 4.7: Visualization depicting the learned pattern of the agent during Phase 1 of the training process. The analysis focuses on the behavior observed in the final three episodes of the Q-Learning process, which spanned 1,000 episodes. During these episodes, the exploration rate is so low that the agent predominantly exploits its accumulated knowledge. The first row illustrates the agent's configuration of the NVM Middleware with high number of interactive threads (approximately 15) and low number of batch threads (approximately 5), aligning with preliminary results for Phase 4. In the middle row, the throughput and 99th percentile latency reported by the NVM Middleware at each time step are depicted. By employing the optimal combination of threads, the agent consistently maintains low latency (less than 250 microseconds) and a throughput exceeding 250,000 operations/second across most steps. Finally, the bottom row illustrates the operations per second sent to the NVM Middleware by Phase 4.
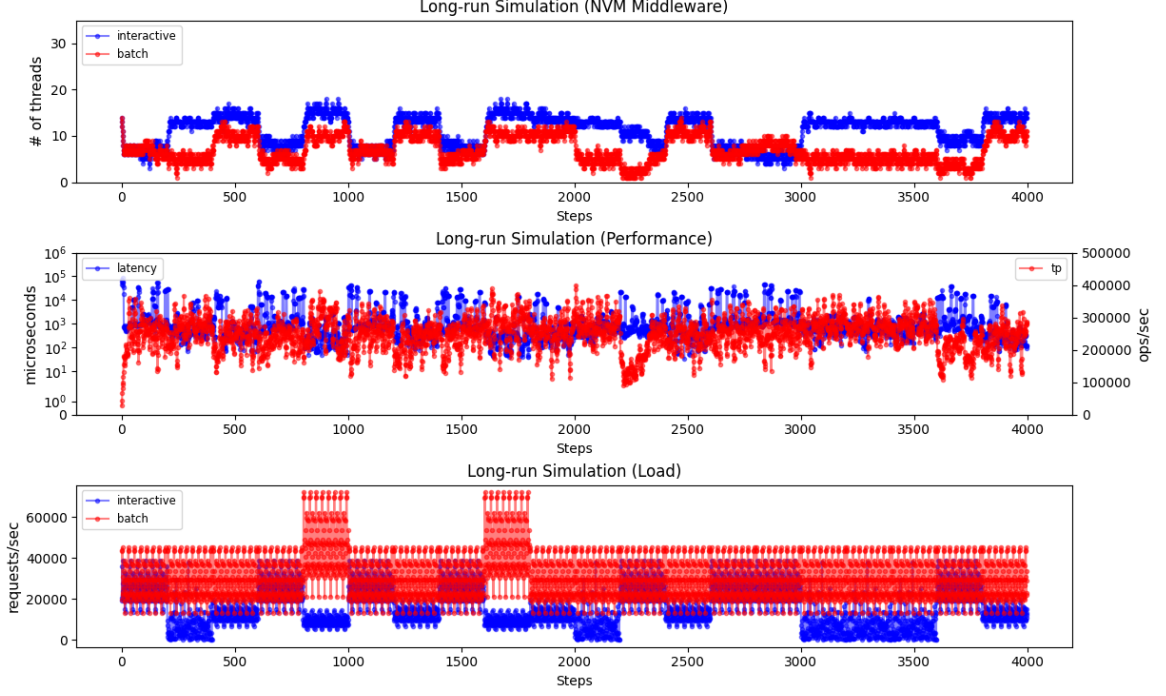
Evaluating the RL Agent

Figure 4.8: Illustration demonstrating the dynamic adjustment of thread counts by the RL agent during a test comprising 4,000 steps with randomly alternating phases. The top row showcases the RL agent's utilization of learned knowledge to optimize the number of interactive and batch threads for each phase. In the middle row, the throughput and 99th percentile latency reported by the NVM Middleware at each time step are depicted. By dynamically modifying the NVM Middleware threads, the throughput aligns with the predefined throughput SLA. However, unexpected spikes in the 99th percentile latency are observed, contrary to the training phase. The bottom row illustrates the operations per second sent by each phase, highlighting the shift in patterns every 200 steps.

We evaluate the trained RL agent's performance against two baseline scenarios: one with disabled concurrency control in the NVM Middleware and another with a fixed policy of 15 interactive and batch threads. Each test comprises a long-run simulation spanning 4,000 steps, with the workload changing every 200 steps. We capture the minimum, 25th, 50th, 75th, and maximum throughput and tail latency observed by the NVM Middleware, as well as the environment rewards for each test. Figure 4.8 illustrates the dynamic behavior

56

of the RL agent as it adapts the combination of interactive and batch threads in response to the current workload patterns learned during training.

Our observations demonstrate the added performance benefits of RL-driven policies under varying workloads. While incorporating the NVM Middleware with a fixed policy yields performance improvements, dynamic control implemented by the RL agent further enhances performance. Increased rewards (Table 4.9) observed by the RL agent indicate superior maximization of performance and adherence to target SLAs. This is reflected in the achieved throughput (Table 4.10), with the NVM Middleware meeting the throughput target for 50% of steps, compared to less than 25% for the fixed policy scenario. Furthermore, although not achieving the target throughput in all steps, the NVM Middleware's overall throughput is closer to the target compared to the other scenarios.

However, in this experiment, the 99th percentile latency (Table 4.11) exhibited by both scenarios using the NVM Middleware did not meet expectations. We attribute this issue to the chosen interactive workloads not sufficiently stressing the system, leading to better performance in the scenario with no concurrency control. Further discussion on this topic is provided in Section 6.

Table 4.9: Analysis of the rewards achieved by the RL agent under shifting workloads compared to two baseline scenarios: one without concurrency control and the other keeping the NVM Middleware threads fixed. The values represent the distribution of reward signals reported by the environment at each time step, ranging from the minimum to the maximum observed, along with quartiles and median scores. Overall, the NVM Middleware with the RL agent achieves the highest reward.

	No NVM Middleware	NVM Middleware Fixed	NVM Middleware + RL
Min	-94,755.386	-65,157.089	-87,907.434
Q1	-10,790.1	-8,605.4625	-3,647.9454
Median	-6,983.235	-3,208.995	-4.005294
Q3	-4,042.9125	-2.353015	0.31523
Max	3.174046	4.89667	4.582787

Table 4.10: Analysis of the throughput achieved by the RL agent under shifting workloads compared to two baseline scenarios: one without concurrency control and the other keeping the NVM Middleware threads fixed. The values represent the distribution of throughput (operations/second) measurements reported by the NVM Middleware at each time step, ranging from the minimum to the maximum observed, along with quartiles and median scores. Overall, the NVM Middleware with the RL agent achieves the highest throughput.

	No NVM Middleware	NVM Middleware Fixed	NVM Middleware + RL
Min	72,218.9	104,719.9	159,168.8
Q1	112,440	148,792.5	218,816.25
Median	135,508.5	186,877	252,078.5
Q3	166,340.25	231,597.75	278,205
Max	242,104.4	357,445.6	352,800.27

Table 4.11: Analysis of the throughput achieved by the RL agent under shifting workloads compared to two baseline scenarios: one without concurrency control and the other keeping the NVM Middleware threads fixed. The values represent the distribution of latency (microseconds) measurements reported by the NVM Middleware at each time step, ranging from the minimum to the maximum observed, along with quartiles and median scores. Surprisingly, in this particular test, both configurations involving the NVM Middleware exhibited higher latency compared to the baseline without concurrency control. This unexpected outcome suggests that the interactive workloads may not have adequately stressed the system, resulting in increased latency when utilizing the NVM Middleware. Further investigation is warranted to ascertain the underlying factors contributing to this behavior.

	No NVM Middleware	NVM Middleware Fixed	NVM Middleware + RL
Min	19	89	130.95
Q1	81	239	396.75
Median	19	674.5	754
Q3	271.5	1,888.75	1,427
Max	82,824	34,090.93	34,712.04

Chapter 5: Related Work

This chapter provides a comprehensive review of the relevant literature within the scope of our study. The literature review is categorized into several domains, including research focusing on resource contention in Optane PMem, studies addressing the constraints of current cloud storage services, and investigations utilizing reinforcement learning for optimizing resource allocation decisions.

Optane PMem Resource Contention: Prior research has highlighted resource contention issues within Optane PMem [12, 14]. Strategies to mitigate these challenges often involve limiting the number of concurrent threads accessing persistent memory. Yang et al. [12] enhance the performance of an PM-aware file system by limiting the number of writer threads per Optane PMem DIMM. Similarly, Li et al. [14] address the overhead incurred by multiple threads flushing data from CPU caches to persistent memory by implementing a runtime system that regulates thread concurrency.

Our work draws inspiration from the approaches mentioned above. We design the NVM Middleware as an integration layer that applies model-guided optimizations to leverage Optane PMem effectively. Similar to Ribbon, our work controls concurrency levels on persistent memory and dynamically adjusts thread counts as necessary. However, the NVM Middleware introduces a novel approach beyond conventional concurrency controls. It implements a workload-aware concurrency mechanism that allocates distinct worker threads for different workload types, enabling performance segregation among workloads with diverse requirements. Furthermore, unlike Ribbon, the NVM Middleware incorporates latency and bandwidth service level agreements to proactively adjust worker thread allocations for each workload type, leveraging reinforcement learning to adapt to workload changes.

Limitations of Existing Cloud Storage Services: Research on serverless platforms has underscored inefficiencies stemming from limitations in existing cloud storage offerings.

Several systems have emerged to alleviate communication bottlenecks in serverless functions [5, 9, 23, 46, 54–56].

Some systems minimize storage overhead by reducing traffic to remote storage and utilizing local communication mechanisms among related serverless functions [23, 55]. SAND [55] facilitates direct communication between related serverless functions running on the same server via a local message bus. FAA$T [23] introduces a transparent and auto-scalable in-memory caching layer to prioritize data reuse and reduce calls to remote storage. Similarly, Cloudburst [56] enhances data locality for serverless functions by implementing a key-value cache on each machine hosting function invocations.

Others focus on tailored storage solutions for data-intensive serverless workloads, bridging performance and capacity gaps between DRAM and persistent storage through multi-tier storage approaches [5, 46]. Pocket [5] utilizes application hints to determine data tier storage, while Anna [46] employs frequency analysis of key invocations to dynamically move data between tiers. These systems employ reactive policies to autoscale resources based on predefined thresholds.

In contrast, the NVM Middleware capitalizes on Optane PMem's unique blend of persistence and memory-like speeds to bridge performance and capacity gaps without necessitating data tiering policies. Moreover, it adopts a proactive approach to resource autoscaling, leveraging Reinforcement Learning to predict workload changes and preemptively adjust resources.

Additionally, Tariq et al. [39] introduced a framework aimed at enhancing the scheduling of serverless function chains to elevate the quality of service provided by serverless platforms. While not storage-centric, this work underscores the importance of improving service quality in serverless environments. Similarly, Pisces [38] extends performance isolation policies by achieving per-tenant performance isolation and fairness in shared storage services, suggesting a potential research direction for enhancing the NVM Middleware.

Reinforcement Learning-based Optimization Policies: Cano et al. [47] introduced a novel application of Reinforcement Learning to enhance task scheduling policies

in their cluster environments. Their approach involved employing linear regression models to approximate the Q-function, a fundamental component in Q-Learning algorithms. Additionally, they conducted offline pre-training of these linear models, guided by model selection and hyper-parameter tuning processes. By initializing the RL agent with pre-trained models, they facilitated a faster learning process by providing initial knowledge about the environment. Inspired by their methodology, we adopted similar strategies in implementing our RL agent and Q-learning process, albeit using polynomial regression models instead.

Chapter 6: Discussions and Future Research

This chapter delves into the limitations inherent in our methodology and the insights gleaned from the findings presented. Subsequently, potential avenues for future research are explored in light of these limitations.

Storage Service Integration: Originally, this thesis aimed to design a simple storage server facilitating communication with applications via Remote Procedure Calls (RPC), leveraging the NVM Middleware to optimize Optane PMem performance. However, our measurements were affected by network overhead in the infrastructure housing the server with Optane PMem. Thus, evaluating the NVM Middleware on a real-world serverless storage service remains a future research endeavor. Anna key-value database [57] proposes a promising option for assessing the NVM Middleware by extending it to incorporate a storage tier based on Optane PMem, thereby utilizing the NVM Middleware as the optimization layer for persistent memory.

Reducing Autoscaling Overhead: Our current approach to scaling resources involves adding or removing up to two threads per 1-second window, which may delay the system's adaptation to the optimal combination of interactive and batch threads. This delay could contribute to performance spikes observed in the results. An intriguing avenue for exploration is enabling the NVM Middleware to add or remove more than two threads per time step to expedite adaptation to workload changes, potentially enhancing SLA fulfillment efficiency. However, this approach may introduce additional actions in the action space, increasing the RL model's complexity.

Choice of Workloads: While YCSB offers versatility in testing various workloads, its simulations may not accurately reflect real-world serverless workload characteristics. Thus, in this thesis, we rely on I/O traces collected from actual serverless platforms to evaluate our RL approach. However, crafting experimental workloads based on real-world

serverless traces, with modified characteristics such as block size and read-to-write ratio, was necessary to test the RL agent's autoscaling capabilities under shifting workloads. Yet, our chosen workloads may have hindered the RL agent's ability to meet latency SLA targets. Obtaining additional real-world serverless I/O traces could shed light on the NVM Middleware's limitations and capabilities. However, acquiring such traces is challenging and time-consuming, as the RL agent must undergo the entire learning process for each stage, from dataset generation for hyperparameter tuning to running Q-learning episodes.

Exploring Other Function Approximation Techniques: When constructing an RL model, feature extraction plays a crucial role, albeit it is complex. While we select relevant features for our RL model, covering more generic use cases may necessitate additional features to enhance learning capabilities. These features could encompass workload characteristics, NVM Middleware metrics, Optane PMem internal metrics, and general server metrics like CPU and memory usage. Limitations in feature representation may impede regression-based function approximators' efficacy [42]. Alternatively, employing deep neural networks for function approximation [58], known as deep reinforcement learning, could address these challenges. Deep reinforcement learning has demonstrated success in complex scenarios by autonomously discovering useful features, as evidenced in gaming environments [59, 60].

Learning Workload Characteristics: The current strategy employed by the NVM Middleware involves utilizing predefined hints regarding workload characteristics to allocate requests to specific queues. However, this approach may encounter scalability challenges, prompting the exploration of autonomous learning methods for workload characteristics. Several approaches can be considered, ranging from straightforward categorization based on predefined criteria to more sophisticated methods leveraging machine learning models.

Optane PMem Optimizations: Beyond the number of concurrent threads accessing persistent memory concurrently, as highlighted by Yang et al., additional factors influence

the performance of Optane PMem. An intriguing avenue for future research involves investigating how these factors impact performance under FaaS workloads and discerning ways to enhance the NVM Middleware to address these supplementary limitations.

Chapter 7: Conclusions

This thesis explored the utilization of Intel Optane DC Persistent Memory (Optane PMem) to serve as a low-latency and high-throughput storage medium for constructing a serverless storage service capable of efficiently managing Function-as-a-Service (FaaS) workloads. Focusing on the inherent limitations of Optane PMem in handling concurrent processes, we analyzed their impact on storage media latency, throughput, and adherence to predefined service level agreements (SLAs) under varying FaaS workloads. Considering the diverse nature of applications within serverless workloads, our investigation concentrated on two distinct application types: interactive applications requiring low latency and batch applications necessitating high throughput. We developed a set of applications to simulate real-world FaaS workloads, aiming to glean insights into optimizing Optane PMem for FaaS usage scenarios.

Our research confirmed that running multi-threaded applications simulating serverless workloads results in degraded latency and throughput performance of persistent memory. Consistent with prior studies, this underscores the necessity of implementing concurrency control mechanisms over Optane PMem. Notably, we found that the performance degradation may disproportionately affect certain applications, depending on their specific performance requirements.

Our findings advocate for a nuanced approach to concurrency control, suggesting the implementation of independent concurrency levels tailored to each application type to mitigate performance interference among interactive and batch applications. Such contention management mechanisms must align with the objectives of an efficient cloud storage service, encompassing transparent autoscaling and the fulfillment of predefined SLAs.

To address these challenges, we propose the development of the NVM Middleware to regulate concurrency levels on Intel PMem, catering to low-latency and high-throughput demands in serverless scenarios involving interactive and batch applications sharing this storage medium. Our experiments demonstrate that the NVM Middleware yields performance benefits compared to scenarios lacking concurrency control or utilizing fixed concurrency levels. Specifically, our middleware's workload-aware concurrency control mechanism has been observed to improve latency and throughput by factors of up to $435x$ and $8x$, respectively, for interactive and batch workloads sharing Optane PMem, compared to scenarios without concurrency control.

Moreover, our research introduces a reinforcement learning (RL) model designed to effectively capture the intricacies of storage media managing requests from FaaS workloads. With this model, we train an RL agent to dynamically adjust the concurrency control mechanisms implemented by the NVM Middleware in response to workload changes, ensuring adherence to predefined SLAs. Our work illustrates that the RL agent surpasses static policy approaches in performance and adherence to predefined SLAs.

In conclusion, this thesis illuminates strategies for optimizing concurrency levels on Optane DC PMem to achieve peak performance when utilized as storage media for FaaS workloads. By comprehending the limitations of Optane PMem and their ramifications on FaaS workloads, we can refine the functionality of the NVM Middleware.

Bibliography

[1] Yu Gan, Yanqi Zhang, Dailun Cheng, Ankitha Shetty, Priyal Rathi, Nayan Katarki, Ariana Bruno, Justin Hu, Brian Ritchken, Brendon Jackson, Kelvin Hu, Meghna Pancholi, Yuan He, Brett Clancy, Chris Colen, Fukang Wen, Catherine Leung, Siyuan Wang, Leon Zaruvinsky, Mateo Espinosa, Rick Lin, Zhongling Liu, Jake Padilla, and Christina Delimitrou. An Open-Source Benchmark Suite for Cloud and IoT Microservices, 2019.

[2] Sadjad Fouladi, Riad S Wahby, Brennan Shacklett, Karthikeyan Vasuki Balasubramaniam, William Zeng, Rahul Bhalerao, Anirudh Sivaraman, George Porter, and Keith Winstein. Encoding, fast and slow:{Low-Latency} video processing using thousands of tiny threads. In *14th USENIX Symposium on Networked Systems Design and Implementation (NSDI 17)*, pages 363–376, 2017.

[3] Vicent Giménez-Alventosa, Germán Moltó, and Miguel Caballer. A framework and a performance assessment for serverless MapReduce on AWS Lambda. *Future Generation Computer Systems*, 97:259–274, 2019.

[4] Benjamin Carver, Jingyuan Zhang, Ao Wang, Ali Anwar, Panruo Wu, and Yue Cheng. Wukong: A scalable and locality-enhanced framework for serverless parallel computing. In *Proceedings of the 11th ACM symposium on cloud computing*, pages 1–15, 2020.

[5] Ana Klimovic, Yawen Wang, Patrick Stuedi, Animesh Trivedi, Jonas Pfefferle, and Christos Kozyrakis. Pocket: Elastic ephemeral storage for serverless analytics. In *13th USENIX Symposium on Operating Systems Design and Implementation (OSDI 18)*, pages 427–444, 2018.

[6] Joao Carreira, Pedro Fonseca, Alexey Tumanov, Andrew Zhang, and Randy Katz. Cirrus: A serverless framework for end-to-end ml workflows. In *Proceedings of the ACM Symposium on Cloud Computing*, pages 13–24, 2019.

[7] Lang Feng, Prabhakar Kudva, Dilma Da Silva, and Jiang Hu. Exploring serverless computing for neural network training. In *2018 IEEE 11th international conference on cloud computing (CLOUD)*, pages 334–341. IEEE, 2018.

[8] Jingyuan Zhang, Ao Wang, Xiaolong Ma, Benjamin Carver, Nicholas John Newman, Ali Anwar, Lukas Rupprecht, Vasily Tarasov, Dimitrios Skourtis, Feng Yan, and Yue Cheng. Infinistore: Elastic serverless cloud storage. *Proc. VLDB Endow.*, 16(7):1629–1642, mar 2023.

[9] Eric Jonas, Johann Schleier-Smith, Vikram Sreekanti, Chia-Che Tsai, Anurag Khandelwal, Qifan Pu, Vaishaal Shankar, Joao Carreira, Karl Krauth, Neeraja Yadwadkar,

et al. Cloud programming simplified: A berkeley view on serverless computing. *arXiv preprint arXiv:1902.03383*, 2019.

[10] Qifan Pu, Shivaram Venkataraman, and Ion Stoica. Shuffling, fast and slow: Scalable analytics on serverless infrastructure. In *16th USENIX symposium on networked systems design and implementation (NSDI 19)*, pages 193–206, 2019.

[11] Intel. Intel Optane Persistent Memory. `https://www.intel.com/content/www/us/en/products/docs/memory-storage/optane-persistent-memory/overview.html`. 2024.

[12] Jian Yang, Juno Kim, Morteza Hoseinzadeh, Joseph Izraelevitz, and Steve Swanson. An empirical guide to the behavior and use of scalable persistent memory. In *18th USENIX Conference on File and Storage Technologies (FAST 20)*, pages 169–182, 2020.

[13] Joseph Izraelevitz, Jian Yang, Lu Zhang, Juno Kim, Xiao Liu, Amirsaman Memaripour, Yun Joon Soh, Zixuan Wang, Yi Xu, Subramanya R Dulloor, et al. Basic performance measurements of the intel optane DC persistent memory module. *arXiv preprint arXiv:1903.05714*, 2019.

[14] Kai Wu, Ivy Peng, Jie Ren, and Dong Li. Ribbon: High performance cache line flushing for persistent memory. In *Proceedings of the ACM International Conference on Parallel Architectures and Compilation Techniques*, pages 427–439, 2020.

[15] Steve Scargall. *Programming Persistent Memory: A Comprehensive Guide for Developers*. Apress, USA, 1st edition, 2020.

[16] Ivy Peng, Kai Wu, Jie Ren, Dong Li, and Maya Gokhale. Demystifying the performance of hpc scientific applications on nvm-based memory systems. In *2020 IEEE International Parallel and Distributed Processing Symposium (IPDPS)*, pages 916–925. IEEE, 2020.

[17] Intel. Solve Modern Data Challenges with Memory Tiering. `https://www.intel.com/content/www/us/en/products/docs/memory-storage/optane-persistent-memory/memory-tiering-improving-data-management-paper.html`. 2024.

[18] Persistent Memory Documentation. `https://docs.pmem.io/persistent-memory/getting-started-guide/introduction`. 2024.

[19] Andy Rudoff. Persistent memory programming. *Login: The Usenix Magazine*, 42(2):34–40, 2017.

[20] Intel. Speeding Up I/O Workloads with Intel Optane Persistent Memory. `https://www.intel.com/content/www/us/en/developer/articles/technical/speeding-up-io-workloads-with-intel-optane-dc-persistent-memory-modules.html`. 2024.

[21] Storage Networking Industry Association. NVM Programming Model. `https://www.snia.org/sites/default/files/technical-work/npm/release/SNIA-NVM-Programming-Model-v1.2.pdf`. 2024.

[22] Intel. pmem/pmemkv: Key/Value Datastore for Persistent Memory. `https://github.com/pmem/pmemkv`. 2024.

[23] Francisco Romero, Gohar Irfan Chaudhry, Íñigo Goiri, Pragna Gopa, Paul Batum, Neeraja J. Yadwadkar, Rodrigo Fonseca, Christos Kozyrakis, and Ricardo Bianchini. Faa$T: A Transparent Auto-Scaling Cache for Serverless Applications, 2021.

[24] Amazon. AWS Lambda. `https://aws.amazon.com/lambda/`. 2024.

[25] Microsoft. Azure Functions. `https://azure.microsoft.com/en-us/products/functions/`. 2024.

[26] Google. Cloud Functions. `https://cloud.google.com/functions`. 2024.

[27] Apache Software Foundation. Apache OpenWhisk. `https://openwhisk.apache.org/`. 2024.

[28] Mohammad Shahrad, Rodrigo Fonseca, Inigo Goiri, Gohar Chaudhry, Paul Batum, Jason Cooke, Eduardo Laureano, Colby Tresness, Mark Russinovich, and Ricardo Bianchini. Serverless in the wild: Characterizing and optimizing the serverless workload at a large cloud provider. In *2020 USENIX annual technical conference (USENIX ATC 20)*, pages 205–218, 2020.

[29] Amazon. AWS S3. `https://aws.amazon.com/s3/`. 2024.

[30] Amazon. Amazon DynamoDB. `https://aws.amazon.com/pm/dynamodb/`. 2024.

[31] Giuseppe DeCandia, Deniz Hastorun, Madan Jampani, Gunavardhan Kakulapati, Avinash Lakshman, Alex Pilchin, Swaminathan Sivasubramanian, Peter Vosshall, and Werner Vogels. Dynamo: Amazon's highly available key-value store. In *ACM Symposium on Operating System Principles*, 2007.

[32] Microsoft. Azure Blob Storage. `https://azure.microsoft.com/en-us/products/storage/blobs`. 2024.

[33] Google. Cloud Storage. `https://cloud.google.com/storage`. 2024.

[34] Google. Datastore. `https://cloud.google.com/datastore`. 2024.

[35] Microsoft. Azure Cosmos DB. `https://azure.microsoft.com/en-us/products/cosmos-db`. 2024.

[36] Public Cloud Object-store Performance is Very Unequal across AWS S3, Google Cloud Storage, and Azure Blob Storage. `https://dev.to/sachinkagarwal/public-cloud-object-store-performance-is-very-unequal-across-aws-s3-google-cloud-storage-and-azure-blob-storage-13do`. 2024.

[37] Amazon. Amazon ElastiCache. `https://aws.amazon.com/pm/elasticache/`. 2024.

[38] David Shue, Michael J. Freedman, and Anees Shaikh. Performance Isolation and Fairness for Multi-Tenant Cloud Storage. In *10th USENIX Symposium on Operating Systems Design and Implementation (OSDI 12)*, pages 349–362, Hollywood, CA, October 2012. USENIX Association.

[39] Ali Tariq, Austin Pahl, Sharat Nimmagadda, Eric Rozner, and Siddharth Lanka. Sequoia: Enabling quality-of-service in serverless computing. In *Proceedings of the 11th ACM symposium on cloud computing*, pages 311–327, 2020.

[40] Richard S Sutton and Andrew G Barto. *Reinforcement learning: An introduction*. MIT press, 2018.

[41] Christopher John Cornish Hellaby Watkins. *Learning from delayed rewards*. PhD thesis, King's College, Cambridge United Kingdom, 1989.

[42] Stuart S Russell and Petter Norvig. *Artificial Intelligence: A Modern Approach*. Pearson, 2020.

[43] Introduction to Linear Regression and Polynomial Regression. `https://towardsdatascience.com/introduction-to-linear-regression-and-polynomial-regression-f8adc96f31cb`. 2024.

[44] James Bergstra and Yoshua Bengio. Random search for hyper-parameter optimization. *Journal of machine learning research*, 13(2), 2012.

[45] Ana Klimovic, Yawen Wang, Christos Kozyrakis, Patrick Stuedi, Jonas Pfefferle, and Animesh Trivedi. Understanding ephemeral storage for serverless analytics. In *2018 USENIX annual technical conference (USENIX ATC 18)*, pages 789–794, 2018.

[46] Chenggang Wu, Vikram Sreekanti, and Joseph M Hellerstein. Autoscaling tiered cloud storage in Anna. *Proceedings of the VLDB Endowment*, 12(6):624–638, 2019.

[47] Ignacio Cano, Srinivas Aiyar, Varun Arora, Manosiz Bhattacharyya, Akhilesh Chaganti, Chern Cheah, Brent Chun, Karan Gupta, Vinayak Khot, and Arvind Krishnamurthy. Curator:{Self-Managing} Storage for Enterprise Clusters. In *14th USENIX Symposium on Networked Systems Design and Implementation (NSDI 17)*, pages 51–66, 2017.

[48] N Marivate Vukosi. *Improved Empirical Methods in Reinforcement Learning Evaluation*. PhD thesis, PhD thesis, Rutgers, New Brunswick, New Jersey, 2015.

[49] Intel. Intel oneAPI Threading Building Blocks. `https://www.intel.com/content/www/us/en/developer/tools/oneapi/onetbb.html#gs.4oc8fg`.

[50] scikit-learn: machine learning in Python. `https://scikit-learn.org/stable/`. 2024.

[51] Wenzel Jakob. pybind11 documentation. `https://pybind11.readthedocs.io/en/stable/index.html`. (Accessed on 02/18/2024).

[52] Yahoo! Cloud Serving Benchmark in C++. `https://github.com/basicthinker/YCSB-C`. 2024.

[53] Microsoft. Azure/AzurePublicDataset: Microsoft Azure Traces. `https://github.com/Azure/AzurePublicDataset`. 2024.

[54] Simon Shillaker and Peter Pietzuch. Faasm: Lightweight isolation for efficient stateful serverless computing. In *2020 USENIX Annual Technical Conference (USENIX ATC 20)*, pages 419–433, 2020.

[55] Istemi Ekin Akkus, Ruichuan Chen, Ivica Rimac, Manuel Stein, Klaus Satzke, Andre Beck, Paarijaat Aditya, and Volker Hilt. {SAND}: Towards {High-Performance} serverless computing. In *2018 Usenix Annual Technical Conference (USENIX ATC 18)*, pages 923–935, 2018.

[56] Vikram Sreekanti, Chenggang Wu, Xiayue Charles Lin, Johann Schleier-Smith, Joseph E. Gonzalez, Joseph M. Hellerstein, and Alexey Tumanov. Cloudburst: stateful functions-as-a-service. *Proceedings of the VLDB Endowment*, 13(12):2438–2452, August 2020.

[57] Chenggang Wu, Jose M Faleiro, Yihan Lin, and Joseph M Hellerstein. Anna: A kvs for any scale. *IEEE Transactions on Knowledge and Data Engineering*, 33(2):344–358, 2019.

[58] Q-learning with Neural Networks. `http://outlace.com/rlpart3.html`. 2024.

[59] Volodymyr Mnih, Koray Kavukcuoglu, David Silver, Alex Graves, Ioannis Antonoglou, Daan Wierstra, and Martin Riedmiller. Playing atari with deep reinforcement learning. *arXiv preprint arXiv:1312.5602*, 2013.

[60] David Silver, Julian Schrittwieser, Karen Simonyan, Ioannis Antonoglou, Aja Huang, Arthur Guez, Thomas Hubert, Lucas Baker, Matthew Lai, Adrian Bolton, et al. Mastering the game of go without human knowledge. *nature*, 550(7676):354–359, 2017.